Effective low-energy description of the two-impurity Anderson model: RKKY interaction and quantum criticality

Fabian Eickhoff,[1] Benedikt Lechtenberg,[2] and Frithjof B. Anders[1]
[1]*Theoretische Physik 2, Technische Universität Dortmund, 44221 Dortmund, Germany*
[2]*Department of Physics, Kyoto University, Kyoto 606-8502, Japan*

(Received 8 June 2018; published 4 September 2018)

We show that the RKKY interaction in the two-impurity Anderson model comprise two contributions: a ferromagnetic part stemming from the symmetrized hybridization functions and an antiferromagnetic part. We demonstrate that this antiferromagnetic contribution can also be generated by an effective local tunneling term between the two impurities. This tunneling can be analytically calculated for particle-hole symmetric impurities. Replacing the full hybridization functions by the symmetric part and this tunneling term leads to the identical low-temperature fixed point spectrum in the numerical renormalization group. Compensating this tunneling term allows us to restore the Varma-Jones quantum critical point between a strong-coupling phase and a local singlet phase even in the absence of particle-hole symmetry in the hybridization functions. We analytically investigate the spatial frequencies of the effective tunneling term based on the combination of the band dispersion and the shape of the Fermi surface. Numerical renormalization group calculations provide a comparison of the distance-dependent tunneling term and the local spin-spin correlation function. Deviations between the spatial dependency of the full spin-spin correlation function and the textbook RKKY interaction are reported.

DOI: 10.1103/PhysRevB.98.115103

I. INTRODUCTION

Using technology based on quantum-mechanical phenomena for efficient computations requires the realization of quantum bits, which might be implemented via quantum impurity systems [1–5]. Magnetic adatoms and molecules on surfaces as well as nanostructured gate controlled devices could serve as the smallest building blocks for such systems [6–19], which allows the combination of traditional electronics with novel spintronics and have been intensively studied in the last decades.

The two-impurity Anderson model (TIAM) provides one of the simplest systems of two independent local moments that indirectly couple through the conduction band of the host or substrate material. It is particularly interesting since it accounts for the competition of two mechanisms [20–35] that influence the magnetic properties of the ground state. For a ferromagnetic Ruderman-Kittel-Kasuya-Yosida (RKKY) [36–38] interaction J_{RKKY}, both impurity spins align parallel and are screened by the itinerant conduction electrons, while for strong antiferromagnetic interactions, both spins form an interimpurity singlet, which decouples from the conduction band.

This observation triggered intensive research in the 1970s and 1980s in the context of heavy fermions [39] since it has been suggested that this competition provides a basic understanding of this class of materials: depending on the interaction strength either a heavy Fermi liquid or a antiferromagnetically ordered ground state is found driven by the local singlet formation [40]. There is an ongoing discussion [41,42] whether the change of ground states in a lattice system is connected to a quantum phase transition [22,43,44] in a two-impurity system.

The transition between these two singlet phases in the TIAM is driven by the ratio between the Kondo temperature T_{K} and J_{RKKY} [40,44–50]. While a quantum critical point (QCP) separates both ground states in the presence of a special kind of particle-hole (P-H) symmetry [22,43,49], the quantum phase transition is replaced by a crossover if that symmetry is broken [51]. Including the energy dependence in the impurity coupling function generally leads to a P-H asymmetric model and, consequently, to a crossover behavior. Therefore the QCP found by Varma and Jones [22,43,44] is a consequence of an oversimplification of the problem [52]. Recently, however, it has been shown [53] that for certain dispersions and distances between the impurities the TIAM exhibits a QCP, separating two orthogonal ground states with different degeneracy. This QCP is of different nature and has been experimentally observed in PTCDA-Au complexes on an Au surface [12] and is driven by the additional direct tunneling term between the two neighboring molecular orbitals [12,53].

In this paper, we derive an analytical, nonperturbative formula, based on a symmetry analysis of the parity dependent and distance-dependent hybridization function, which allows to map the emerging scattering terms onto an effective tunneling $t^{\mathrm{eff}}(\vec{R})$ between the impurities. We present a full numerical renormalization group (NRG) calculation [54–57] to prove the equivalence of the effective and the original two-impurity problem.

The construction of the effective tunneling term provides a new insight to the nature of the AF contribution to the RKKY interaction. For the wide-band limit, we find that the AF contribution to J_{RKKY} is determined by $(t^{\mathrm{eff}})^2/U$, where U denotes the Coulomb interaction. This result is contrary to a separate two-step transformation: (i) a Schrieffer-Wolff

transformation [58] onto the two-impurity Kondo model and (ii) the perturbative calculation of J_{RKKY} using this two-impurity Kondo model, which would predict a $1/U^2$ dependency. Only at very large values of U, where charge fluctuations are strongly suppressed, the characteristic energy scale crosses over to the $1/U^2$ textbook expression. The distance dependence of the effective tunneling term can explain our numerical findings that the impurity spin-spin correlation function decays remarkably slower than the textbook expression of the RKKY interaction, even for a finite bandwidth of the conduction band. We study the spatial anisotropy of this tunneling term on a simple cubic lattice and find a surprising direct connection between slow (fast) spatial oscillations and particle (hole) doping, that is, beyond the standard $2k_{\mathrm{F}}$ oscillations.

The understanding of the effective tunneling term enables us to engineer the recovery of the Varma and Jones quantum critical point in the TIAM for arbitrary distances, even for a particle-hole symmetry broken model that generically only shows a continuous change of the conduction electron scattering phase. Such additional local tunneling term can also naturally occur in neighboring molecular orbitals as shown by density functional theory [12].

This paper is structured as follows. We start by defining the model, its mapping onto the parity eigenbasis and the fixed point (FP) structure of the NRG level flow in Sec. II. In Sec. III, we review the different types of P-H symmetries and derive the effective low-temperature description of the model, based on an additional spatial-dependent local tunneling term $t^{\mathrm{eff}}(\vec{R})$. This approach is applied in Sec. IV to restore the QCP of Varma and Jones by investigating the impurity spectral functions, the scattering phase of the Green function, and the NRG level flow. We also cover the finite distance and finite bandwidth corrections to the impurity spin-spin correlation function. Section V is devoted to the analytical analysis of the spatial frequencies governing the spatial anisotropy of the spin-spin correlation function in a simple cubic lattice as a function of the chemical potential, and, therefore, the shape of the Fermi surface. We close with a summary in Sec. VI.

II. THEORY

A. Two-impurity Anderson model

The Hamiltonian of the TIAM can be divided into three parts:

$$H_{\mathrm{TIAM}} = H_{\mathrm{imp}} + H_{\mathrm{host}} + H_{\mathrm{hyb}}. \tag{1}$$

The impurity part is given by

$$H_{\mathrm{imp}} = \sum_{l\in\{1,2\},\sigma} \epsilon_l^f f_{l,\sigma}^\dagger f_{l,\sigma} + \frac{t}{2}\sum_{l,\sigma} f_{l,\sigma}^\dagger f_{\bar{l},\sigma} + \frac{1}{2}\sum_{l\in\{1,2\},\sigma} U_l f_{l,\sigma}^\dagger f_{l,\sigma} f_{l,\bar{\sigma}}^\dagger f_{l,\bar{\sigma}}. \tag{2}$$

The operator $f_{l,\sigma}^{(\dagger)}$ destroys (creates) an electron with spin $\sigma = \pm$ on impurity l, whose onsite energy is labeled by ϵ_l^f. U denotes the onsite Coulomb repulsion. Furthermore, we also allow for a tunneling term t between both impurities. Such a hopping term is realized in a system where the local orbitals are given by the lowest unoccupied molecular orbitals of two neighboring molecule complexes that start to overlap at short distance and form dimers [12].

The metallic host is described by a free conduction band

$$H_{\mathrm{host}} = \sum_{\vec{k},\sigma} \epsilon_{\vec{k}}^c c_{\vec{k},\sigma}^\dagger c_{\vec{k},\sigma}, \tag{3}$$

where $c_{\vec{k}}(c_{\vec{k}}^\dagger)$ is the annihilation (creation) operator of an electron in the conduction band with dispersion $\epsilon_{\vec{k}}^c$. The interaction between the impurities and the host accounted for by

$$H_{\mathrm{hyb}} = \sum_{\substack{l\in\{1,2\}\\ \vec{k},\sigma}} (V_{l\vec{k}} c_{\vec{k},\sigma}^\dagger e^{i\vec{k}\vec{R}_l} f_{l,\sigma} + \mathrm{H.c.}). \tag{4}$$

Here, $V_{l\vec{k}}$ denotes the hybridization of the impurity located at position $\vec{R}_l$ with the conduction band state $\vec{k}$.

In the following, we consider the parity symmetric case, $V_{1\vec{k}} = V_{2\vec{k}} = V_{\vec{k}}$, $\varepsilon_0^f = \epsilon_1^f = \epsilon_2^f$; $U_1 = U_2$, unless stated otherwise. Close to integer valence of one electron per impurity, a local moment is formed at intermediate temperatures [58] that is screened for $T \to 0$ [20,21,55]. This is the case for $\varepsilon_0^f \approx -U/2 < 0$ and will be the main focus of this paper.

The hybridization induces an effective Heisenberg exchange interaction, the RKKY interaction, between the two impurities that alters in sign with the characteristic spatial dependency of $\cos(2k_F R)/R^d$ for $Rk_{\mathrm{F}} \gg 1$ with d being the spatial dimension of the host, assuming a simplified energy dispersion of the conduction band.

We can also add an additional direct Heisenberg exchange interaction $J_{12}\vec{S}_1\vec{S}_2$ to the full two-impurity Hamiltonian

$$H'_{\mathrm{TIAM}}(J_{12}) = H_{\mathrm{TIAM}} + J_{12}\vec{S}_1\vec{S}_2 \tag{5}$$

as an external control parameter for the investigation of the QCP of the Varma-Jones (VJ) type [21].

B. Energy representation of the TIAM Hamiltonian

It is convenient to convert to a site-dependent and energy-dependent operator [51,54], defining

$$c_{l,\sigma}(\varepsilon) = \sqrt{\frac{\pi}{\Gamma(\epsilon)}} \sum_{\vec{k}} V_{\vec{k}} \delta\big(\epsilon - \epsilon_{\vec{k}}^c\big) e^{i\vec{k}\vec{R}_l} c_{\vec{k},\sigma}, \tag{6}$$

where the hybridization function $\Gamma(\epsilon)$,

$$\Gamma(\epsilon) = \pi \sum_{\vec{k}} |V_{\vec{k}}|^2 \delta\big(\epsilon - \epsilon_{\vec{k}}^c\big), \tag{7}$$

is determined from the equal-site anticommutator $\{c_{l,\sigma}(\varepsilon), c_{l,\sigma'}^\dagger(\varepsilon')\} = \delta_{\sigma\sigma'}\delta(\varepsilon - \varepsilon')$.

The hybridization takes the form

$$H_{\mathrm{hyb}} = \sum_{l\in\{1,2\}} \int_{-D}^{D} d\varepsilon \sqrt{\frac{\Gamma(\epsilon)}{\pi}} f_{l,\sigma}^\dagger c_{l,\sigma}(\varepsilon) + \mathrm{H.c.} \tag{8}$$

in the continuum limit, with the bandwidth $2D$ of the host.

Using the effective hybridization matrix element V given by

$$\int_{-D}^{D} d\varepsilon \Gamma(\epsilon) = V^2 \pi, \tag{9}$$

we can define an effective conduction band density of states (DOS), $\rho(\varepsilon) = \Gamma(\varepsilon)/(\pi V^2)$.

The operators $c_{l,\sigma}(\varepsilon)$ are connected to the same single conduction band and are not linearly independent. Therefore they are combined into parity eigenstates [12,20,22,43,51,59,60] with even (e) and odd (o) parity that anticommute by symmetry. The spatial dependence in this even-odd parity basis is included in the new orthogonal energy-dependent field operators

$$c_{\mu,\sigma}(\varepsilon) = \sqrt{\frac{\pi}{\Gamma_\mu(\epsilon)}} \sum_{\vec{k}} V_{\vec{k}} \delta\big(\epsilon - \epsilon^c_{\vec{k}}\big)\big(e^{i\frac{\vec{k}\vec{R}}{2}} + s_\mu e^{-i\frac{\vec{k}\vec{R}}{2}}\big) c_{\vec{k},\sigma}, \tag{10}$$

with $\mu \in \{e, o\}$, $\vec{R} = \vec{R}_1 - \vec{R}_2$ and $s_e = 1$, $s_o = -1$. The effective hybridization functions,

$$\begin{aligned} \Gamma_e(\epsilon, \vec{R}) &= \pi \sum_{\vec{k}} |V_{\vec{k}}|^2 \delta\big(\epsilon - \epsilon^c_{\vec{k}}\big) \cos^2(\vec{k}\vec{R}/2), \\ \Gamma_o(\epsilon, \vec{R}) &= \pi \sum_{\vec{k}} |V_{\vec{k}}|^2 \delta\big(\epsilon - \epsilon^c_{\vec{k}}\big) \sin^2(\vec{k}\vec{R}/2), \end{aligned} \tag{11}$$

are defined such that the standard anticommutation relations $\{c_{\mu,\sigma}(\varepsilon), c^\dagger_{\mu',\sigma'}(\varepsilon')\} = \delta(\epsilon - \epsilon')\delta_{\mu,\mu'}\delta_{\sigma,\sigma'}$ are fulfilled. They determine the effective coupling of the two different flavors even and odd to the impurity and obey the sum rule

$$\Gamma(\varepsilon) = \Gamma_e(\varepsilon, \vec{R}) + \Gamma_o(\varepsilon, \vec{R}). \tag{12}$$

Introducing an even/odd parity basis also for the impurity operators,

$$f_{\mu,\sigma} = \frac{1}{\sqrt{2}}(f_{1,\sigma} + s_\mu f_{2,\sigma}), \tag{13}$$

yields a flavor diagonal hybridization between the impurities and these even/odd conduction bands:

$$H_{\text{hyb}} = \sum_{\mu\in\{e,o\},\sigma} \int_{-D}^{D} d\epsilon \sqrt{\frac{\Gamma_\mu(\varepsilon, \vec{R})}{2\pi}} c^\dagger_{\mu,\sigma}(\varepsilon) f_{\mu,\sigma} + \text{H.c.} \tag{14}$$

By extracting the effective flavor coupling constant V_μ,

$$V^2_\mu(\vec{R})\pi = \int_{-D}^{D} d\varepsilon \Gamma_\mu(\epsilon, \vec{R}), \tag{15}$$

we define the effective DOS of the flavor bands by normalization [57,61],

$$\bar{\rho}_\mu(\varepsilon, \vec{R}) = \frac{1}{V^2_\mu(\vec{R})\pi} \Gamma_\mu(\epsilon, \vec{R}). \tag{16}$$

One can always find a proper normalized $\bar{\rho}_o(\varepsilon, \vec{R})$ in the limit $\vec{R} \to 0$: the decoupling of the odd conduction band is accounted for by $V_o \to 0$. To this end, the hybridization can be expressed as

$$H_{\text{hyb}} = \sum_{\mu\sigma} V_\mu(\vec{R}) \int_{-D}^{D} d\epsilon \sqrt{\bar{\rho}_\mu(\varepsilon, \vec{R})} c^\dagger_{\mu,\sigma}(\varepsilon) f_{\mu,\sigma} + \text{H.c.}, \tag{17}$$

separating the coupling strength to the impurity from the energy dependency of a normalized conduction band used to construct the semi-infinite Wilson chains [20,22,43,51,57,59,60]. Note that the energy dependence of $\bar{\rho}_\mu(\varepsilon)$ generally destroys P-H symmetry.

The transformation of the local Coulomb interaction,

$$H_U = \frac{1}{2} \sum_{l\in\{1,2\},\sigma} U_l f^\dagger_{l,\sigma} f_{l,\sigma} f^\dagger_{l,\bar{\sigma}} f_{l,\bar{\sigma}}, \tag{18}$$

from the real space basis to the even/odd basis introduced in Eq. (13) generates a large exchange interaction $J = U/2$ as well as a corresponding pair-hopping term required for maintaining the SU(2) spin symmetry—for details see Ref. [12]. This pair hopping term conserves the parity but violates the flavor conservation in the even and odd channel similar to the flavor violating term of the TIKM in Ref. [21].

Low temperature fixed points

In this section, we briefly review the known low-temperature FP structure of the TIAM model [20,22,43,51,57]. Since we are interested in the competition between the Kondo effect and the singlet formation due to the RKKY interaction, we focus on the regime of single occupancy of each impurity orbital.

Starting from a single-impurity Anderson model in a parameter regime where the Schrieffer-Wolff transformation [58] is applicable, the low-temperature FP is given by a strong-coupling (SC) FP describing the Kondo effect. The crossover to this FP is governed by a nonanalytic energy scale T_{K} that is exponentially small in terms of the bare coupling constants. The local spin of the magnetic impurity is dynamically screened by the conduction electrons and the remaining conduction electron degrees of freedom decouple from the impurity. Thus the SC FP agrees with that of a free electron gas (FEG) with one electron removed that forms the Kondo singlet. The conduction electrons close to the Fermi energy acquire a phase shift δ in accordance with Friedel's sum rule [62,63].

While P-H symmetry pins the phase shift to $\delta = \pi/2$, P-H asymmetry leads to potential scattering in the conduction band which changes the phase shift continuously. The SC FP Hamiltonian

$$H^{\text{SC}}(K) = H^{\text{SC}}_{\text{PH}} + K \sum_\sigma (\bar{c}^\dagger_{0\sigma} \bar{c}_{0\sigma} - 1) \tag{19}$$

is given [55,56] by a P-H symmetric term $H^{\text{SC}}_{\text{PH}}$ and a marginal operator breaking P-H symmetry that is parameterized by the constant K. The operators $\bar{c}_{n\sigma}$ annihilate an electron with spin σ on site $n = 0, 1, \ldots$ of the semi-infinite Wilson chain. All other scattering terms are irrelevant. Below, we will make use of the fact that the FP is fully characterized by a single constant K defining a line of renormalization group (RP) FPs [55,56].

For the two-impurity Kondo model, the effective RKKY interaction [21] is given by the expression

$$J_{\mathrm{RKKY}}^{\mathrm{Kondo}} = \int_{-D}^{0} d\epsilon \int_{0}^{D} d\epsilon'\, \rho(\epsilon)\rho(\epsilon')\frac{J^2}{16} \times \left(\frac{N_e^2(\epsilon)N_e^2(\epsilon') + N_o^2(\epsilon)N_o^2(\epsilon')}{\epsilon - \epsilon'} - \frac{N_e^2(\epsilon)N_o^2(\epsilon') + N_o^2(\epsilon)N_e^2(\epsilon')}{\epsilon - \epsilon'} \right) \tag{20}$$

in the limit $T \to 0$, where the dimensionless normalization functions $N_{e(o)}(\varepsilon)$ are defined as

$$N_e^2(\varepsilon) = \frac{4}{N\rho(\varepsilon)} \sum_{\vec{k}} \delta(\varepsilon - \varepsilon_{\vec{k}}) \cos^2\left(\frac{\vec{k}\vec{r}}{2}\right), \qquad N_o^2(\varepsilon) = \frac{4}{N\rho(\varepsilon)} \sum_{\vec{k}} \delta(\varepsilon - \varepsilon_{\vec{k}}) \sin^2\left(\frac{\vec{k}\vec{r}}{2}\right), \tag{21}$$

and $\rho(\epsilon)$ is the DOS of the original conduction band prior to the mapping onto the even and odd basis—see Ref. [59] for details. In order to understand the low-temperature FP of the TIAM, we start from the Varma-Jones approximation [21] and neglect the energy dependency: $N_\mu^2(\epsilon) \to N_\mu^2$ as well $\bar{\rho}_\mu(\varepsilon) \to \rho_0$, enforcing P-H symmetry of both DOS. Then (20) reduces to Eq. (7) in Ref. [21],

$$H_{\mathrm{RKKY}} = J_{\mathrm{RKKY}}^{\mathrm{Kondo}} \vec{S}_1 \vec{S}_2 = (8 \ln 2)\rho_0 (J_e - J_o)^2 \vec{S}_1 \vec{S}_2, \tag{22}$$

where $J_e(J_o)$ is the Kondo coupling to the even (odd) channel after the basis transformation—for a detailed derivation of this expression see the appendix of Ref. [59].

Since only a FM RKKY interaction is dynamically generated by this simplification, an additional local spin-spin coupling $J_{12}\vec{S}_1\vec{S}_2$ has been added by the authors of Ref. [21] by hand in order to access the AF RKKY regime. For a large FM $(-J_{12}) \gg 0$, the locally favored triplet is screened by both conduction electron flavors via a two-stage Kondo effect since generally $V_o \neq V_e$. The FP is given by $H_{\mathrm{PH}}^{\mathrm{SC}}$ and $\delta_\mu = \pi/2$. For a large antiferromagnetic (AF) coupling, $J_{12} \gg 0$, a local singlet is favored and the RG FP is given by those of a free electron gas $H_{\mathrm{PH}}^{\mathrm{FEG}}$ and $\delta_\mu = 0$. Since P-H symmetry is only compatible with these two scattering phases, there must be a critical AF coupling at which the SC Kondo phase is replaced by the local singlet phase [51]. This quantum critical point (QCP) occurs at $J_{12}/T_K \approx 2.2$ [22,43]. Once the full energy dependency of $\bar{\rho}_\mu(\varepsilon)$ required for the correct description of the RKKY interaction is taken into account, the Varma-Jones QCP is replaced by a smooth crossover [45].

III. DERIVATION OF THE EFFECTIVE TUNNELING TERM

Now we derive an analytical counter term to the bare Hamiltonian that allows to restore the Varma-Jones QCP for arbitrary impurity distances. The naive strategy would be to add a suitable potential scattering term to the conduction electrons to restore P-H symmetry at the FP [64]. The parameter $\bar{K}_\mu$, however, is subject to an RG flow, and it is very cumbersome to iteratively determine $\bar{K}_\mu$. In addition, the physical insight gained from such a term is limited.

It turns out that modifying the tunneling term in H_{imp} defined in Eq. (2) has an identical effect and the required t^{eff} can be analytically derived from the coupling functions $\Gamma_\mu(\varepsilon, \vec{R})$. There are essentially two scenarios. (i) If the impurities are P-H symmetric ($\epsilon_l = -U/2$), there is a strong symmetry restriction of the type of potential scattering counter term. In this case, the low-temperature FP becomes P-H symmetric and $\delta_e = \delta_o = \pi/2$. (ii) Local P-H asymmetry on the impurities generates potential scattering in at least one of the channels. Although we can modify these scattering terms to achieve $\delta_e = \delta_o$, which is sufficient to restore the Varma-Jones QCP [51,65], the scattering phases differ from $\pi/2$. Since the parameters necessary to restore the QCP can be analytically derived only for the first scenario, we start with $\epsilon_l = -U/2$ and come back to the second case latter.

A. Particle-hole symmetry and potential scattering

We now review the connection between P-H symmetry and the arising potential scattering terms discussed by Affleck *et al.* [51]. The TIAM with P-H symmetric impurities can exhibit two different types of particle-hole symmetries. The first type of P-H transformation requires a flavor diagonal transformation

$$c_{\mu,\sigma}(\varepsilon) \to c_{\mu,\sigma}^\dagger(-\varepsilon) \tag{23}$$

and is a symmetry of the Hamiltonian if the effective conduction bands are compatible with

$$\bar{\rho}_\mu(-\epsilon, \vec{R}) = \bar{\rho}_\mu(\epsilon, \vec{R}). \tag{24}$$

However, the system can also be invariant under the second, flavor exchanging P-H transformation

$$c_{e/o,\sigma}(\varepsilon) \to c_{o/e,\sigma}^\dagger(-\varepsilon) \tag{25}$$

if $V_\mu^2(\vec{R})\bar{\rho}_\mu(-\epsilon, \vec{R})$ satisfy the relations

$$V_e^2(\vec{R})\bar{\rho}_e(-\epsilon, \vec{R}) = V_o^2(\vec{R})\bar{\rho}_o(\epsilon, \vec{R}). \tag{26}$$

In general, the potential scattering terms generated in higher order of perturbation theory takes the form

$$H_{\mathrm{s}} = \sum_{\mu\in\{e,o\}} \int_{-D}^{D} \mathrm{d}\epsilon \mathrm{d}\epsilon' [S_\mu(\epsilon, \epsilon')c_\mu^\dagger(\varepsilon)c_\mu(\varepsilon')]. \tag{27}$$

If the original problem is P-H symmetric, the effective potential scattering term must also satisfy the special type of symmetry transformation. Depending on the type of P-H symmetry, we require

$$\begin{aligned} &\text{first type} \longrightarrow S_{e/o}(\epsilon, \epsilon') = -S_{e/o}(-\epsilon, -\epsilon'), \\ &\text{second type} \longrightarrow S_{e/o}(\epsilon, \epsilon') = -S_{o/e}(-\epsilon, -\epsilon'), \end{aligned} \tag{28}$$

thus the scattering function must vanish at zero energy in the presence of the first type of symmetry, whereas the second type only requires a connection between the even and odd channels:

$$\begin{aligned} &\text{first type} \longrightarrow S_{e/o}(0, 0) = 0, \\ &\text{second type} \longrightarrow S_{e/o}(0, 0) = -S_{o/e}(0, 0). \end{aligned} \tag{29}$$

Since the zero-energy scattering terms in the even and odd channels in general lead to different phase shifts $\delta_{e/o}$ and hence destroy the QCP, only the first type of P-H symmetry ensures the existence of a QCP in the TIAM automatically.

B. Low energy description and effective tunneling

Even for a P-H symmetric dispersion $\epsilon^c_{\vec{k}}$ of the original problem, the effective DOS $\bar{\rho}_\mu(\varepsilon, \vec{R})$ defined in Eq. (16) will generally not comply with any of the two types of P-H symmetries. However, one can divide $\bar{\rho}_\mu(\varepsilon, \vec{R})$ into the two contributions

$$\bar{\rho}^{(\pm)}_\mu(\varepsilon, \vec{R}) = \tfrac{1}{2}[\bar{\rho}_\mu(\varepsilon, \vec{R}) \pm \bar{\rho}_\mu(-\varepsilon, \vec{R})], \tag{30}$$

while $\bar{\rho}^{(+)}_\mu(\varepsilon, \vec{R})$ satisfies Eq. (24) and is normalized.

$\bar{\rho}^{(-)}_\mu(\varepsilon, \vec{R})$ has a vanishing integral spectral weight and, therefore, cannot be interpreted as an effective bath. This term breaks the P-H symmetry of first type and contributes to the scattering terms.

Consequently, the Hamiltonian of each conduction band flavor μ can be decomposed into

$$H_{\text{host},\mu} = H^+_{\text{host},\mu} + \Delta H^-_{\text{host},\mu}\,, \tag{31}$$

where $H^+_{\text{host},\mu}$ describes a fictitious bath with P-H symmetry of the first type, while $\Delta H^-_{\text{host},\mu}$ stems from redistribution of spectral weight due to $\bar{\rho}^{(-)}_\mu(\varepsilon, \vec{R})$ that can be accounted for by an appropriately chosen scattering function $S_\mu(\epsilon, \epsilon')$ in Eq. (27).

We make use of the fact [55,56,64] that the P-H symmetry breaking leads to a modification of the fixed point Hamiltonian controlled by a single scattering parameter K_μ in each band, such that we alternatively can approximate the host by

$$H_{\text{host},\mu} \approx H^+_{\text{host},\mu} + K_\mu \sum_\sigma (\bar{c}^\dagger_{0\mu\sigma}\bar{c}_{0\mu\sigma} - 1)\,. \tag{32}$$

If $\rho(\epsilon)$, as defined below Eq. (9), is invariant under energy inversion, i.e., $\rho(\epsilon) = \rho(-\epsilon)$, one can show that $V^2_e(\vec{R})\bar{\rho}^{(-)}_e(-\varepsilon, \vec{R}) = -V^2_o(\vec{R})\bar{\rho}^{(-)}_o(\varepsilon, \vec{R})$. As a consequence, $K_e = -K_o$ or $K_\mu = s_\mu K$, and the problem is reduced to a single parameter that determines the low-temperature effect of $\bar{\rho}^{(-)}_e(\varepsilon, \vec{R})$.

Now we turn to the full Hamiltonian of the TIAM that also contains the local impurity degrees of freedom and the coupling between both subsystems. An impurity interaction that is invariant under the transformation

$$\begin{aligned} & f_{e/o,\sigma} \to f^\dagger_{o/e,\sigma} \\ \Leftrightarrow \quad & f_{1,\sigma} \to f^\dagger_{1,\sigma}\,; \quad f_{2,\sigma} \to -f^\dagger_{2,\sigma}, \end{aligned} \tag{33}$$

but not under the transformation

$$\begin{aligned} & f_{e/o,\sigma} \to f^\dagger_{e/o,\sigma} \\ \Leftrightarrow \quad & f_{1/2,\sigma} \to f^\dagger_{1/2,\sigma} \end{aligned} \tag{34}$$

is only compatible with the second type of P-H transformation and hence inevitably generates potential scattering terms in the form of $K_e = -K_o \neq 0$ in the low-energy FP that is compatible to Eq. (29). Therefore we can replace the scattering terms in Eq. (32) by an effective impurity interaction $H^{\text{eff}}_{\text{imp}}$ that leads to the same low-energy FP. Note that the invariance of $H^{\text{eff}}_{\text{imp}}$ under the transformations of Eq. (34) ensures that the full Hamiltonian in Eq. (32) remains P-H asymmetric.

The only parity-conserving single-particle term involving only impurity degrees of freedom that is invariant under local P-H transformation of the second type, Eq. (33), but not under (34) is given by

$$\begin{aligned} \mathrm{H}^{\text{eff}}_{\text{imp}} &= \frac{t^{\text{eff}}}{2}\sum_\sigma (f^\dagger_{e,\sigma} f_{e,\sigma} - f^\dagger_{o,\sigma} f_{o,\sigma}) \\ &= \frac{t^{\text{eff}}}{2}\sum_\sigma (f^\dagger_{1,\sigma} f_{2,\sigma} + f^\dagger_{2,\sigma} f_{1,\sigma}). \end{aligned} \tag{35}$$

This term is parameterized by a single parameter t^{eff} that has a simple physical interpretation. It describes an additional electron tunneling term between the two impurities and is fully compatible with H_{imp}. Mahmoud *et al.* already mentioned the existence of such an effective charge exchange in the noninteracting two-impurity Anderson model on a lattice [66].

C. Estimate of effective tunneling

One of the key messages of this paper is that one can subtract an appropriately chosen local impurity counter term $\mathrm{H}^{\text{eff}}_{\text{imp}}$ in order to restore the Varma-Jones QCP. It is well established [45,51] that the QCP is destroyed only by scattering terms compatible with the P-H symmetry of the second kind, leading to different scattering phases in the even and the odd channel. The goal of the counter term is to produce an identical scattering phase $\delta_e = \delta_o$ for $T, \omega \to 0$.

In order to gain some insight and actually calculate t^{eff} in a certain limit, we demand that the low-temperature FP of the full model H_{TIAM} augmented with a counter term $H^{\text{eff}}_{\text{imp}}$,

$$H^{\text{eff}}_{\text{TIAM}} = H_{\text{TIAM}} - H^{\text{eff}}_{\text{imp}}, \tag{36}$$

is identical to those of the effective model $H^+_{\text{TIAM}} \stackrel{!}{=} H^{\text{eff}}_{\text{TIAM}}$ where the full DOS $\bar{\rho}_\mu(\varepsilon, \vec{R})$ in Eq. (17) has been replaced by $\bar{\rho}^{(+)}_\mu(\varepsilon, \vec{R})$ of Eq. (30). If the parameters of the impurities are P-H symmetric, i.e., $\varepsilon^f_0 + U/2 = 0$, the scattering phases of H^+_{TIAM} are distance independent and equal $\delta_e = \delta_o = \pi/2$ and likewise in $H^{\text{eff}}_{\text{TIAM}}$.

The phase shifts at the Fermi energy can be extracted from the local single-particle Green functions. For the full problem including the counter term, the Green function takes the form

$$G_\mu(z, \vec{R}) = \left(z - \varepsilon^f_0 - \Delta_\mu(z, \vec{R}) - \Sigma^U_\mu(z) + s_\mu \frac{t^{\text{eff}}}{2}\right)^{-1}, \tag{37}$$

where $\Sigma^U_\mu(z) = \Sigma^U_\mu[G]$ denotes the correlation self-energy that is given by a functional of the Green function [67], and

$$\Delta^\pm_\mu(z, \vec{R}) = V^2_\mu(\vec{R}) \int_{-D}^{D} d\omega \frac{\bar{\rho}^{(\pm)}_\mu(\omega, \vec{R})}{z - \omega}, \tag{38}$$

$$\begin{aligned} \Delta_\mu(z, \vec{R}) &= \int_{-D}^{D} \frac{d\omega}{\pi} \frac{\Gamma_\mu(\omega, \vec{R})}{z - \omega} \\ &= \Delta^{(+)}_\mu(z, \vec{R}) + \Delta^{(-)}_\mu(z, \vec{R})\,. \end{aligned} \tag{39}$$

For $T \to 0$, the spectral function always takes the form [62,63]

$$\rho_\mu^f(0,\vec{R}) = \lim_{\delta\to 0}\frac{1}{\pi}\Im G_\mu(0-i\delta,\vec{R}) = \frac{1}{\pi\Gamma_\mu(0)}\sin^2\delta_\mu \tag{40}$$

relating the scattering phase δ_μ,

$$\cot(\delta_\mu) = \frac{\varepsilon_0^f + \Re\Delta_\mu(0) + \Re\Sigma_\mu^U(0) - s_\mu\frac{t^{\text{eff}}}{2}}{\Gamma_\mu(0)}, \tag{41}$$

to the ratio of the real and imaginary part of the inverse Green function [62,63]. Note that the Fermi-liquid property $\Im\Sigma^U(0\pm i\delta) = 0$ at $T = 0$ has entered as well as a coupling $|\Gamma_\mu(0)| > 0$.

In general, this a complicated problem determining t^{eff} by the condition $\delta_\mu = \text{const}$. Therefore we restrict ourselves to a locally P-H symmetric impurity $\varepsilon_0^f + U/2 = 0$ that implies a Hartree term $\Re\Sigma^U(0) = U/2$. Since $\delta_\mu = \pi/2$ independent of $\Gamma_\mu(0)$, the nominator must vanish, which leads to the condition

$$t^{\text{eff}}(\vec{R}) = 2s_\mu V_\mu^2(\vec{R})\int_{-D}^{D} d\omega\frac{\bar{\rho}_\mu(\omega,\vec{R})}{\omega} = 2s_\mu\Re(\Delta_\mu(0,\vec{R})) = 2s_\mu\Re(\Delta_\mu^{(-)}(0,\vec{R})). \tag{42}$$

In order to set the stage for the full NRG calculations below, we assume a constant DOS $\rho(\varepsilon) = \rho_0 = 1/2D$ and an isotropic linear dispersion $\epsilon_{\vec{k}}^c = v_{\text{F}}(|\vec{k}| - k_{\text{F}})$, where v_{F} is the Fermi velocity and k_{F} the Fermi wave vector. The evaluation of Eq. (11) can be performed analytically [22,43,59,60] for different spatial dimensions

$$\text{1d}: V_\mu^2(\vec{R})\bar{\rho}_\mu(\varepsilon,\vec{R}) = 2V^2\rho_0\left\{1 + s_\mu\cos\left[Rk_{\text{F}}\left(1+\frac{\epsilon}{D}\right)\right]\right\}, \tag{43}$$

$$\text{2d}: V_\mu^2(\vec{R})\bar{\rho}_\mu(\varepsilon,\vec{R}) = 2V^2\rho_0\left\{1 + s_\mu J_0\left[Rk_{\text{F}}\left(1+\frac{\epsilon}{D}\right)\right]\right\}, \tag{44}$$

$$\text{3d}: V_\mu^2(\vec{R})\bar{\rho}_\mu(\varepsilon,\vec{R}) = 2V^2\rho_0\left\{1 + s_\mu\frac{\sin\left[Rk_{\text{F}}\left(1+\frac{\epsilon}{D}\right)\right]}{Rk_{\text{F}}\left(1+\frac{\epsilon}{D}\right)}\right\}, \tag{45}$$

where $R = |\vec{R}|$ is the absolute distance between the impurities, V^2 is defined in Eq. (9), and $J_0(x)$ denotes the zeroth Bessel function of the first kind. We defined $\Gamma_0 = V^2\pi\rho_0$ and plot the effective hopping parameter $t^{\text{eff}}(R)$ as a function of the dimensionless distance $x = Rk_{\text{F}}/\pi$ for different spatial dimensions in Fig. 1.

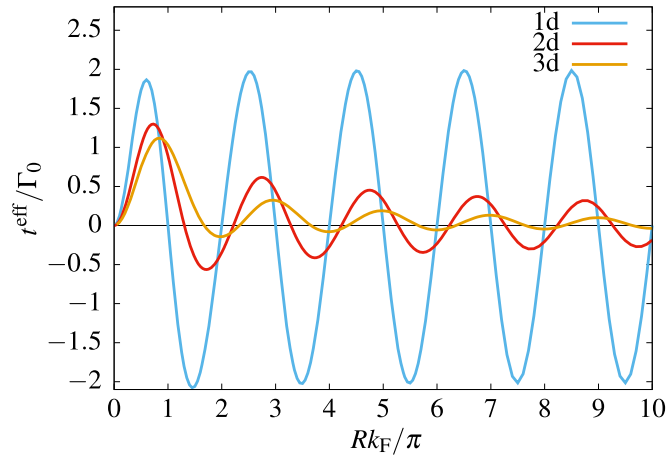

FIG. 1. Effective hopping element t^{eff} for different spatial dimensions d as a function of the dimensionless distance Rk_{F}/π.

IV. APPLICATION OF THE EFFECTIVE TUNNELING TERM

A. Study of the low-temperature fixed point

The effective scattering terms generated by the P-H asymmetric DOSs $\bar{\rho}_\mu^-(\epsilon,\vec{R})$ influence the fixed point spectrum of the full Hamiltonian H_{TIAM} in Eq. (1). For the analysis the distance dependence of these scattering terms, we examine the fixed point properties of the full Hamiltonian H_{TIAM} in Eq. (1), the P-H symmetric fraction H_{TIAM}^+ in Eq. (36) and the FEG H_{host} in Eq. (3) by means of NRG [54–57] in the P-H symmetric case $\varepsilon_f + U/2 = 0$.

Figure 2 shows the low-temperature NRG FP spectrum for a two-dimensional host as a function of the dimensionless distance $x = Rk_{\text{F}}/\pi$ and at odd iteration for the interacting Hamiltonians and even iteration of the FEG. Since the odd conduction band decouples for $R \to 0$ [12,25,47], the level flow of H_{TIAM} matches those of H_{TIAM}^+ that is very different to the flow of the FEG. This FP is well understood: only one half of the local triplet state can be screened by the conduction electrons and the system remains in an underscreened Kondo fixed point [12,25,47,53].

In this paper, however, we will focus on finite distances. The low-temperature FP spectrum of H_{TIAM}^+ at odd iterations coincides with those of the free electron gas at even iterations in contrast to those of the full Hamiltonian where the influence of the effective potential scattering terms lifts the degeneracies caused by the P-H symmetry of H_{TIAM}^+. The periodic structure of the fixed point spectrum of the full Hamiltonian as a function of distance traces the oscillation of $t^{\text{eff}}(\vec{R})$ defined by Eq. (42), which is also added to Fig. 2 as red solid curve. Note that those distances where $t^{\text{eff}}(\vec{R})$ vanished, the FP spectra of H_{TIAM} matches the one for the P-H symmetric free electron gas.

In order to check the accuracy of the predicted effective hopping element, we need to prove that $t^{\text{eff}}(\vec{R})$ is able to compensate the scattering terms due to P-H asymmetry in $\bar{\rho}_\mu(\epsilon,\vec{R})$ so that the FP spectra of $H_{\text{TIAM}} - H_{\text{imp}}^{\text{eff}}$ and H_{TIAM}^+ become identical. These two FP spectra are depicted in Fig. 3. The oscillations of the energy levels disappear in $H_{\text{TIAM}} - H_{\text{imp}}^{\text{eff}}$ as a consequence of the counter term $H_{\text{imp}}^{\text{eff}}$ and both fixed point spectra coincide up to NRG discretization errors that would require a small correction of analytically calculated t^{eff} in order to obtain a perfect cancellation.

The single-particle spectral function of the impurities depicted in Fig. 4 proves the restoring of the P-H symmetry around the Fermi energy by adding the additional counter term. In the absence of the counter term, the spectral function (black line) is asymmetric and the Kondo peak is split [23,47,68] as can be seen in the inset of Fig. 4. By

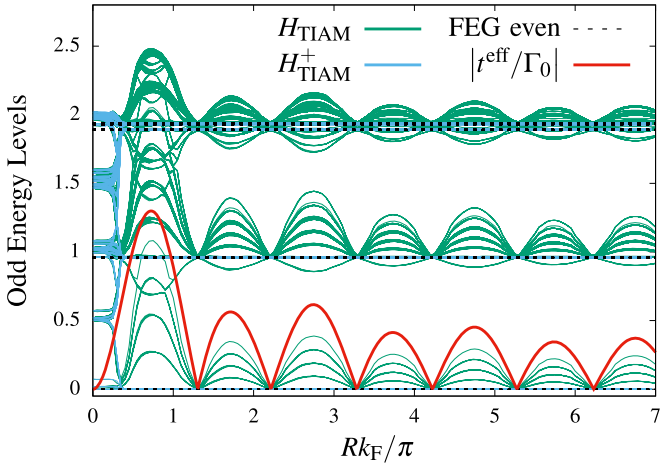

FIG. 2. Low-temperature fixed point spectrum for an odd number of NRG iterations as a function of the dimensionless distance $x = Rk_{\mathrm{F}}/\pi$ for an isotropic linear dispersion $\epsilon^{c}_{\vec{k}}$ in two dimensions. Comparison between the full Hamiltonian (green line), the symmetric fraction (blue line), and the free electron gas (dashed line). In the strong-coupling fixed point, the energy levels corresponding to an odd number of iterations are comparable with the even ones from the free electron gas, since one conduction electron degree of freedom is locked into a singlet with the impurity electron [22,43]. NRG parameters are discretization parameter $\Lambda = 1.5$, number of the kept states $\mathrm{N_s} = 4000$, $U/\Gamma_0 = 10$, $\epsilon^{f}/\Gamma_0 = -5$, $t/\Gamma_0 = 0$, and $D/\Gamma_0 = 10$.

compensating the intrinsic, effective tunneling, the splitting of the Kondo resonance vanishes (light blue line).

B. Restoring the Varma and Jones quantum critical point

1. Local P-H symmetry on the impurities

The Varma and Jones (VJ) QCP is inevitably stable in the presence of the P-H symmetry of the first type, as becomes

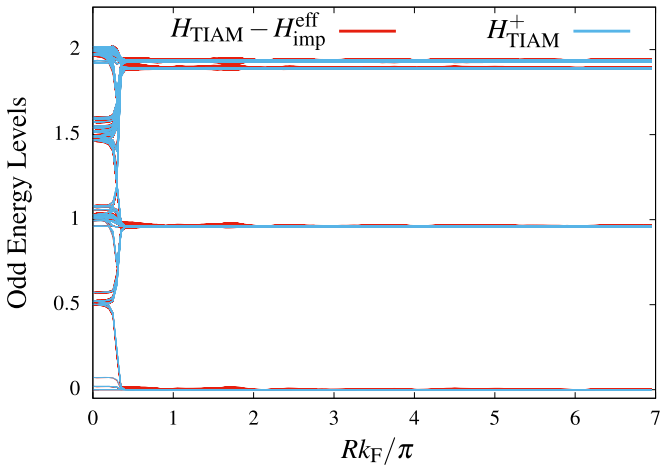

FIG. 3. Low-temperature fixed point spectrum for an odd number of NRG iterations as a function of the dimensionless distance $x = Rk_{\mathrm{F}}/\pi$ for an isotropic linear dispersion $\epsilon^{c}_{\vec{k}}$ in two dimensions. Comparison between the full Hamiltonian minus the effective tunneling (red line) and the symmetric fraction (blue line). NRG parameters as in Fig. 2.

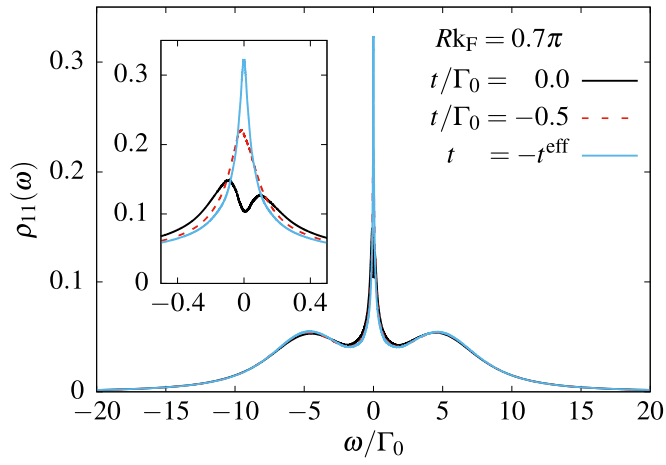

FIG. 4. One-particle spectral function of the impurities for different tunneling parameters and a spatial separation of $Rk_{\mathrm{F}}/\pi = 0.7$ on a two dimensional surface. The effective tunneling $t^{\mathrm{eff}}(Rk_{\mathrm{F}}/\pi = 0.7) = -1.2954\Gamma_0$ leads to an P-H asymmetric gap formation around $\omega = 0$ that can be effaced with an additional hopping element $t = -t^{\mathrm{eff}}$. NRG parameters as in Fig. 2 but with $\Lambda = 2$ and $D/\Gamma_0 = 30$.

apparent by describing the Fermi-liquid phase in terms of the phase shifts in the even and odd channels at zero energy [51]. Making use of the symmetry transformation (23) in combination with the boundary conditions for incoming and outgoing conduction electrons,

$$c^{(\dagger)\,\mathrm{out}}_{e/o}(\epsilon) = e^{(-)2i\delta_{e/o}} c^{(\dagger)\,\mathrm{in}}_{e/o}(-\epsilon), \tag{46}$$

pins the possible phase shift to $\delta_{e/o} = 0 \vee \pi/2$. As a result, there is a QCP separating the Kondo-screening phase ($\delta_{e/o} = \pi/2$) and the interimpurity singlet phase ($\delta_{e/o} = 0$), whereas absence of the P-H symmetry of the first type allows a general phase shift $\delta_{e/o} \in [0, \pi/2]$ with a smooth crossover from 0 to $\pi/2$.

In the preceding section, Sec. IV A, we established the restoration of the P-H symmetry of the first kind in the FP spectrum by a counter $H^{\mathrm{eff}}_{\mathrm{imp}}$. For a vanishing t^{eff}, the FP of $H^{\mathrm{eff}}_{\mathrm{TIAM}}$ turns out to be already P-H symmetric.

In order to prove the presence of the QCP, we added a direct Heisenberg exchange interaction $J_{12}\vec{S}_1\vec{S}_2$ to the full two-impurity Hamiltonian,

$$H'_{\mathrm{TIAM}}(J_{12}) = H_{\mathrm{TIAM}} + J_{12}\vec{S}_1\vec{S}_2. \tag{47}$$

Figure 5(a) depicts three different FP level spectra as a function of J_{12}: for $Rk_F/\pi = 1.2$ with (red dashed line) and without (light blue solid line) a counter term and at the special distance $Rk_F/\pi = 1.30925$ (black solid line). In accordance with the literature, the transition from the Kondo regime ($J_{12} \to -\infty$) to the interimpurity singlet regime ($J_{12} \to \infty$) is continuous for a generic distance such as $Rk_F/\pi = 1.2$ [blue lines in Fig. 5(a)] without an additional counter term.

As demonstrated by the FP spectra, the Varma-Jones QCP can be restored by adding a direct tunneling $t^* = -t^{\mathrm{eff}}(R)$. The level flow jumps discontinuously from one to another FP spectrum at a critical coupling J^{c}_{12} revealing clearly the QCP. Evaluating Eq. (42) for this distance yields $t^*(Rk_F/\pi = 1.2)/\Gamma_0 = -0.2915$.

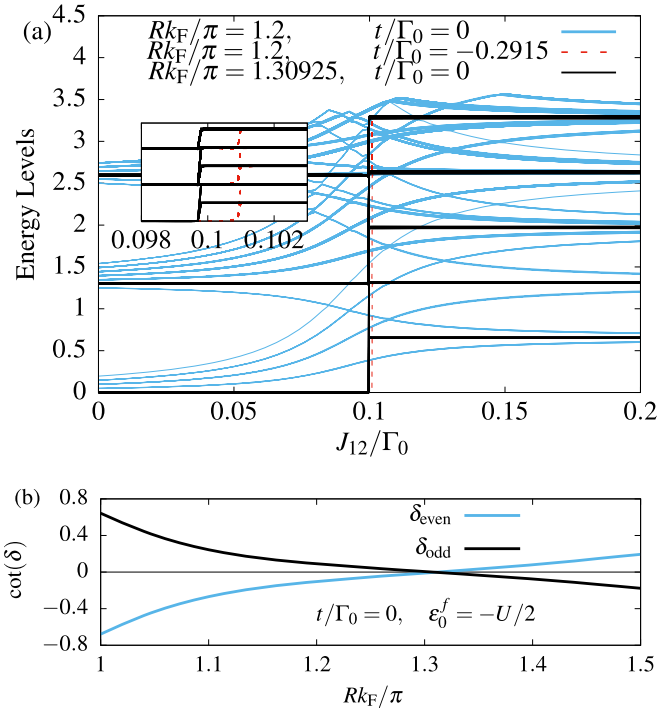

FIG. 5. (a) Development of the low-temperature fixed point spectrum with increasing antiferromagnetic interimpurity spin exchange J_{12}/Γ_0 in two dimensions. A smooth crossover appears for a general P-H asymmetric Hamiltonian with $t = 0$ and $t^{\rm eff}(R) \neq 0$ (blue lines) by contrast with a quantum phase transition for the special case $t^* + t^{\rm eff}(R) = 0$ (red lines) as well as $t = 0$ and $t^{\rm eff}(R^*) = 0$ (black lines). The inset depicts a zoom around the critical value J_{12}^c/Γ_0. (b) Scattering phase in the even and odd channels for a P-H symmetric impurity, plotted against the impurity distance. The QCP exists for $\delta_e = \delta_o = \pi/2$ at $R \approx 1.30925$. NRG parameters as in Fig. 2 but with $\Lambda = 2$.

Alternatively, the distance can be varied to values R^* such that $t^{\rm eff}(R^*)$ vanishes and hence $\cot\delta_e = \cot\delta_o = 0$. Figure 5(b) shows the distance dependency of the scattering phase using the model parameters of Fig. 2. We determined the shortest finite distance for which this condition is fulfilled as $R^* k_F/\pi \approx 1.30925$. For this distance R^*, we scan the FP level flow as a function of J_{12} and add the results to Fig. 5(a) as solid black line. Clearly, we also find a QCP at almost the same critical value for J_{12}. The inset in Fig. 5(a) resolves the very small distance dependent shift of the critical value compared to the case of the generic distance $Rk_F/\pi = 1.2$ with the additional counter term.

2. Local P-H asymmetry on the impurities

Now we proceed to the generic case where also the local P-H symmetry on the impurities is broken but the parity remains conserved. For a fixed U, the single-particle energy is given by the onsite energy $\epsilon^f = -U/2 + \Delta\epsilon$ where $\Delta\epsilon$ parameterized its deviation from the P-H symmetric point. Leaving $\epsilon_0^f = -U/2$, the addition term

$$H_{\Delta\epsilon} = \Delta\epsilon \sum_\sigma (f_{e,\sigma}^\dagger f_{e,\sigma} + f_{o,\sigma}^\dagger f_{o,\sigma}) \tag{48}$$

accounts for the local P-H asymmetry on the impurities. It leads to potential scattering parameter in the form of $K_e \neq -K_o$. Since the absolute value of the scattering terms in the even and in the odd channel does not coincide, it is not possible to cancel both terms simultaneously by introducing a direct tunneling term or varying the spatial separation.

We will demonstrate that the VJ QCP can be restored by changing the low-energy scattering terms such that they generate identical scattering phases in the even and the odd channel, i.e., $\delta_e = \delta_o$. Zhu and Varma [65] pointed out that the scattering phase acquires an additional contribution $\Delta\delta_\mu = \tan^{-1}(\pi\rho_0 K_\mu)$ in the SC FP caused by a P-H asymmetry.

Since neither $\Delta\delta_\mu$ nor K_μ is directly accessible in the NRG, we use a different strategy that is directly based on the NRG FP spectra. Close to the P-H symmetric point, the difference between the lowest single-particle excitation relative to the NRG ground state, E_μ^1, with an even parity ($\mu = e$) and an odd parity ($\mu = o$),

$$\Delta\omega_0 = E_e^1 - E_o^1, \tag{49}$$

is proportional to the difference of the phase shifts.

Tuning the interimpurity spin exchange J_{12} generically drives the system continuously from a SC to a local singlet FP and $\Delta\omega_0$ changes continuously. For a sharp transition, $\Delta\omega_0$ must vanish at the critical coupling J_{12}^c,

$$J_{12}' = \lim_{\delta\to 0} \left(J_{12}^c + \delta\right). \tag{50}$$

Note that the phase shifts at $J_{12} = J_{12}^c$ are not defined. Since the critical value J_{12}^c is unknown *a priori*, it leads to the self-consistency condition

$$\Delta\omega_0(\Delta\epsilon, R^*, t^*, U, J_{12}') = 0. \tag{51}$$

This equation is solved iteratively.

As a starting point, we choose the critical value J_{12}^c for the local P-H symmetric case, i.e., $\Delta\varepsilon = 0$. Then we compute $\Delta\omega_0$ as a function of R (t, respectively) and determine the roots for R_1^* (t_1^*) for constant t (R, respectively). In the next step, we determine the $J_{12}'^2$ at the midpoint of the crossover regime. Inserting $J_{12}'^2$ into Eq. (51) results in new $R_2^*(t_2^*)$. This steps are iterated until convergence is achieved. Starting at the critical distance $R_1^* = 1.30925\pi/k_F$, obtained for $\Delta\epsilon = 0$, $U/\Gamma_0 = 10$, and $t/\Gamma_0 = 0$ in Sec. IV B 1, this procedure converged after four iterations to $R^* k_{\rm F} = 1.24049\pi$ to a precision of five digits.

Figure 6(a) displays the even and odd scattering phases in the last iteration, i.e., for the critical spin exchange J_{12}^c as a function of the distance. This convincingly demonstrates the consistency of our approach. Fixing the last value of J_{12}^c, the point of coincidence of the two scattering phases agrees perfectly with the critical $R^*(\Delta\epsilon/\Gamma_0 = -2)k_{\rm F} = 1.24049\pi$ obtained by the iteration procedure.

In order to prove that the VJ QCP is really restored for this set of parameters, we present the FP level flow as a function of the coupling J_{12} in Fig. 6(b) for the starting distance starting distance $R_1^* k_{\rm F} = 1.30925\pi$ (blue lines) and the final distance R^* (black lines). While only a crossover is observed for R_1^*, clearly the VP QCP is restored at the final distance R^* even for $\Delta\epsilon/\Gamma_0 = -2$. The additional term $t^{\rm eff}$ is not needed. Note the FP level flow in both phases: the different magnitude of

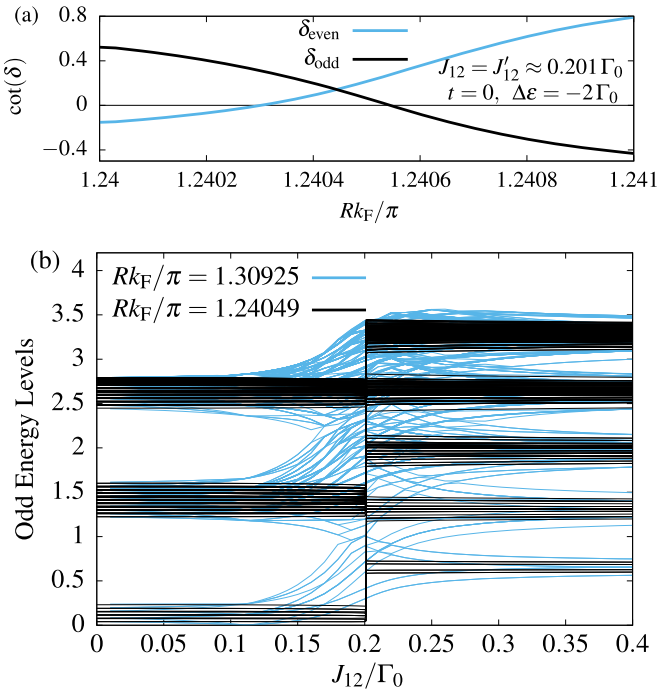

FIG. 6. (a) Scattering phase in the even and odd channel for a P-H asymmetric impurity as a function of R. (b) Low-temperature FP spectrum as a function of J_{12}/Γ_0 and $\Delta\epsilon/\Gamma_0 = -2$ for $R^*(\Delta\epsilon = 0)k_F = 1.30925\pi$ (blue lines) and $R^*(\Delta\epsilon = -2)k_F = 1.24049\pi$ (black lines). NRG parameters as in Fig. 5.

the P-H symmetry breaking scattering term in both phases is clearly visible.

C. Splitting of the RKKY interaction in two contributions

The RKKY interaction between two local moments with a distance R apart is mediated by the metallic host. This effective coupling constant J_{RKKY} is distance dependent and shows the characteristic alternating signs with $2k_F$ oscillations—at least for a simplified dispersion of the conduction electrons.

Consequently, we can divide the RKKY interaction into two contributions with opposite signs. Extending the argument for a constant DOS [21,59] one can show that a P-H symmetric effective DOS $\bar{\rho}^{(+)}(\varepsilon)$ can only generate a ferromagnetic RKKY interaction $J^{\mathrm{FM}}_{\mathrm{RKKY}}$ at arbitrary distances as illustrated by Eqs. (20)–(22). Hence the antiferromagnetic contribution results from the breaking of the P-H symmetry of the first type that can be parameterized by a local t^{eff}.

Decoupling of the impurities from the effective conduction electrons allows for an exact solution of this effective two-impurity problem. For $t^{\mathrm{eff}} = 0$, the local triplet state involving both even and odd orbital is degenerate with the singlet state given by the linear combination of both electrons in the even or both electrons in the odd state [12]. A finite t^{eff} induces an imbalance between the mixing of these singlet states and an energy gain of $J_{\mathrm{ex}} = |t^{\mathrm{eff}}|^2/U > 0$ that can be interpreted as effective interaction between the two local spins in the local moment regime. Clearly, this local exchange mechanism always generates an antiferromagnetic interaction.

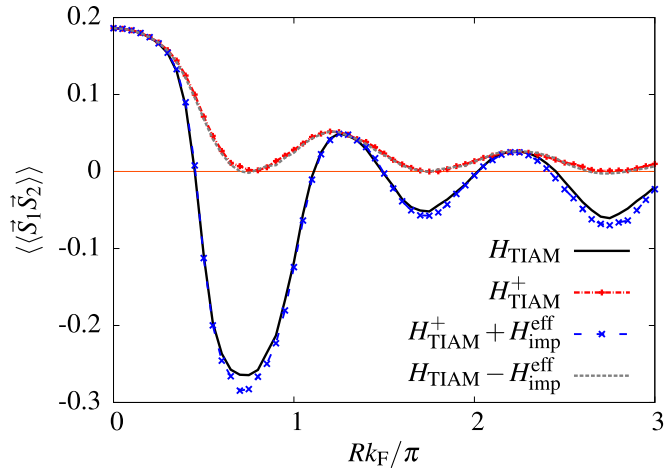

FIG. 7. Impurity spin-spin correlation function as a function of the distance for the full TIAM Hamiltonian, for the effective model and the symmetric part H^+_{TIAM}. A featureless symmetric conduction band with a 2d linear dispersion has been used for the locally P-H symmetric regime for $T \to 0$. Parameters are $U/\Gamma_0 = 10$, $D/\Gamma_0 = 100$, $\mathrm{N_s} = 4000$, and $\Lambda = 2$.

For the local P-H symmetric case, the analytic solution (42) predicts $t^{\mathrm{eff}} \propto \rho_0 V^2$, and the Schrieffer-Wolff transformation [58] generates a local Kondo coupling $J_K \propto V^2/U$. Therefore the local exchange term can be related to J_K via

$$J_{\mathrm{ex}} = \frac{|t^{\mathrm{eff}}|^2}{U} \propto U(\rho(0)J_K)^2. \tag{52}$$

This is a generalization of the $R \to 0$ analysis of FM RKKY in an multi-impurity model [69] to AF contributions for arbitrarily distances R. The estimated order of magnitude of $J_{\mathrm{ex}} \propto 1/U$ agrees perfectly with the cumbersome evaluation of a Rayleigh-Schrdinger perturbation theory in forth order [69]. Our analysis provides a much simpler understanding of the difference of the RKKY interaction in the two-impurity Anderson model and in the two-impurity Kondo model.

Combining these two terms yields the total RKKY coupling $J_{\mathrm{RKKY}} = J^{\mathrm{FM}}_{\mathrm{RKKY}} + J_{\mathrm{ex}}$. This leads to the interesting fact that by adding an additional interimpurity orbital hopping term t, it is possible to change the sign of the total coupling J_{RKKY} in arbitrary direction. Typically, a tunneling term only generates a AF exchange interaction, however, adding a t with opposite sign compared to t^{eff} reduces the total tunneling $\bar{t}^{\mathrm{eff}} = t^{\mathrm{eff}} + t$ and may eventually cause a sign change to a FM J_{RKKY}. On the other side, starting from $t^{\mathrm{eff}} = 0$, i.e., a purely FM J_{RKKY} and increasing t, induces a AF coupling that become arbitrarily large and eventually will also lead to a sign change.

To illustrate that the full energy-dependent TIAM can be mapped to an effective model at low energies comprising an P-H symmetric conduction band, generating the FM RKKY interaction, as well as a local hopping term, which induces the AF part $J^{\mathrm{AF}}_{\mathrm{RKKY}}$, the impurity spin-spin correlation function of both models, calculated by means of the NRG, is shown in Fig. 7. The correlation function $\langle\langle \vec{S}_1 \vec{S}_2 \rangle\rangle$ for H^+_{TIAM} is purely positive demonstrating that the RKKY interaction $J^{\mathrm{FM}}_{\mathrm{RKKY}}$ for a P-H symmetric DOS can only be FM [21]. The correlation

function of the effective model $H^{+}_{\mathrm{TIAM}} + H^{\mathrm{eff}}_{\mathrm{imp}}$ agrees excellently with those of the full model in the short distance regime. We discuss the corrections, which occur for larger distances due to a finite bandwidth, in the next section.

Note that there are infinitely many distances R^{*}_{n} at which $t^{\mathrm{eff}} = 0$, so that $J_{\mathrm{RKKY}} = J^{\mathrm{FM}}_{\mathrm{RKKY}}$ holds. At these distances, the spin-spin correlation function of all models coincided, and the full energy-dependent model with an additional direct spin-spin interaction J_{12} exhibits the VJ QCP.

Note that the effective tunneling t^{eff}, which restores the P-H symmetric FP $H^{+}_{\mathrm{TIAM}} = H_{\mathrm{TIAM}} - H(t^{\mathrm{eff}})$, and the one that restores the FP of the full Hamiltonian out of the P-H symmetric fraction $H_{\mathrm{TIAM}} = H^{+}_{\mathrm{TIAM}} + H(t^{\mathrm{eff}})$, in general are not fully identical. While for a P-H symmetric FP, only the value at zero frequency is relevant, and, consequently, Eq. (42) is exact, corrections stemming from the derivative $d\bar{\rho}_{\mu}(\varepsilon)/d\varepsilon$ need to be taken into account to recover the FP of the full Hamiltonian.

1. Finite bandwidth corrections

Focusing for a moment on a 1d conduction band with a linear dispersion, we noticed that the amplitude of the correlation function of the effective model $H^{+}_{\mathrm{TIAM}} + H^{\mathrm{eff}}_{\mathrm{imp}}$ will not decay for t^{eff} given by Eq. (42). At the distances $R_n k_{\mathrm{F}} = (2n+1)\pi/2$, the Hamiltonian is P-H symmetric of the second type: the symmetric fraction of the effective DOS $\bar{\rho}^{+}_{\mu}(R_n, \varepsilon)$ is constant and distance independent. Furthermore, the effective tunneling is given by the analytical expression

$$t^{\mathrm{eff}}_{1d}(R_n) \propto \int_{-1}^{1} \frac{\sin(R_n k_{\mathrm{F}} x)}{x} dx = 2\mathrm{Si}(R_n k_{\mathrm{F}}), \tag{53}$$

where $\mathrm{Si}(R_n k_{\mathrm{F}})$ is the sine integral, which is constant for large distances $\mathrm{Si}(\infty) = \pi/2$. Apparently, the effective model cannot capture the decay of the impurity spin-spin correlation function for large distances and corrections to the effective model need to be taken into account.

To estimate the magnitude of the corrections, we analyze the resonant level model ($U = 0$), where we can derive an analytic expression for the correlation function. One can show that the correlation function is proportional to the difference of the distance-dependent occupation of the even impurity orbital $n_e(\vec{R})$ and the odd impurity orbital $n_o(\vec{R})$,

$$\langle\langle \vec{S}_1 \vec{S}_2 \rangle\rangle^{U=0} = -\tfrac{3}{8}[n_o(\vec{R}) - n_e(\vec{R})]^2 . \tag{54}$$

At zero temperature these occupation numbers are given by the integral of the analytically obtained spectral functions

$$n_{\mu}(\vec{R}) = \int_{-\infty}^{0} \frac{d\omega}{\pi} \frac{\Gamma_{\mu}(\omega, \vec{R})}{(\omega - \Re(\Delta_{\mu}(\omega, \vec{R})))^2 + \Gamma^2_{\mu}(\omega, \vec{R})}, \tag{55}$$

where the real and imaginary parts of the hybridization function can be decomposed into the contributions from both symmetry types: $\Gamma_{\mu}(\omega) = \Gamma^{+}_{\mu}(\omega) + \Gamma^{-}_{\mu}(\omega)$ and $\Delta_{\mu}(\omega) = \Delta^{+}_{\mu}(\omega) + \Delta^{-}_{\mu}(\omega)$.

In order to derive corrections, we turn to the wide-band limit. We can always find the lowest D such that $\tilde{\varepsilon}_{\vec{k}} = \varepsilon_{\vec{k}}/D \in [-1, 1]$ defines a dimensionless band structure. From Eq. (11), it is clear that the energy dependence of $\Gamma_{\mu}(\omega)$ and $\Re(\Delta_{\mu}(\omega))$ can be expressed through the dimensionless functions $f_{\mu}(\omega/D)$ and $F_{\mu}(\omega/D)$: $\Gamma_{\mu}(\omega) = \Gamma_0 f_{\mu}(\omega/D)$, $\Re(\Delta_{\mu}(\omega)) = \Gamma_0 F_{\mu}(\omega/D)$ and the occupation number can be written as

$$n_{\mu}(\vec{R}) = \int_{-\infty}^{0} \frac{d\omega}{\pi\Gamma_0} \frac{f_{\mu}\left(\frac{\omega}{D}, \vec{R}\right)}{\left(\frac{\omega}{\Gamma_0} - F_{\mu}\left(\frac{\omega}{D}, \vec{R}\right)\right)^2 + \left(f_{\mu}\left(\frac{\omega}{D}, \vec{R}\right)\right)^2}. \tag{56}$$

For fixed hybridization strength Γ_0, and $\Gamma_0/D \to 0$, the total spectral weight is located around

$$\omega_{0,\mu} \approx \Gamma_0 F_{\mu}(0) + \mathcal{O}\left(\frac{\Gamma_0}{D}\right), \tag{57}$$

where we can neglect the correction in the wide-band limit $D \to \infty$.

In the effective Hamiltonian, we include the contributions $\Gamma^{+}_{\mu}(\omega)$ and $\Re\Delta^{+}_{\mu}(\omega)$ exact, but $\Gamma^{-}_{\mu}(\omega)$ and $\Re\Delta^{-}_{\mu}(\omega)$ only up to zero order. In a Taylor series, the leading corrections are generated by the derivatives of these functions. Since

$$\frac{d}{d\omega}\Re(\Delta^{-}_{\mu}(z))\big|_{\omega=0} \propto P\int_{-1}^{1} \frac{\Gamma^{-}(x)}{x^2} dx = 0 , \tag{58}$$

where $x = \omega/D$, the leading corrections are proportional to $\frac{d}{d\omega}\Gamma^{-}_{\mu}(\omega)|_{\omega=0}$, at least for small coupling strengths U/Γ_0. The distance dependence enters in $\frac{d}{d\omega}\Gamma^{-}_{\mu}(\omega)|_{\omega=0}$ differently for different spatial dimensions, but is always proportional to Γ_0/D. For a linear dispersion, we obtain analytically

$$\text{1d}: \quad \frac{d}{d\omega}\Gamma^{-}_{\mu}(\omega)\big|_{\omega=0} \propto \frac{Rk_{\mathrm{F}}\Gamma_0}{D} , \tag{59}$$

$$\text{2d}: \quad \frac{d}{d\omega}\Gamma^{-}_{\mu}(\omega)\big|_{\omega=0} \propto \frac{\sqrt{Rk_{\mathrm{F}}}\Gamma_0}{D} , \tag{60}$$

$$\text{3d}: \quad \frac{d}{d\omega}\Gamma^{-}_{\mu}(\omega)\big|_{\omega=0} \propto \frac{\Gamma_0}{D} . \tag{61}$$

In the limiting case of an infinite bandwidth $\Gamma_0/D \to 0$, the effective tunneling determines the AFM part of the RKKY interaction on all length scales in any dimension.

These theoretical considerations are backed by a comparison of analytical calculations for the two-impurity resonant level model ($U = 0$) in Fig. 8(a) and a full NRG study of the spin-spin correlation function for a finite $U/\Gamma_0 = 10$ in Fig. 8(b) in 1d. Figure 8 shows the correlation as a function of $x = (R_n k_{\mathrm{F}}\Gamma_0)/(\pi D) \propto d\Gamma^{-}_{1\mathrm{d},\mu}/d\omega(\omega = 0)$. In order to extract the power-law of the universal corrections, we logarithmically plot the antiferromagnetic correlation function normalized to its maximum value of -0.75. Panel (a) depicts the evaluation of Eq. (54) for the resonant level model, whereas panel (b) shows the results for the TIAM at finite U/Γ_0, calculated via the NRG. The figure combines the scans for many different values of the band width at the discrete distance $R_n k_{\mathrm{F}} = (2n+1)\pi/2$. Although the effective tunneling is nearly constant, the universality with respect to the scaling variable x is clearly demonstrated. For $x \to 0$, the correlation function approaches a finite value above its theoretical minimum. While the correlation function is constant for small x the corrections become clearly visible for $0.1 < x$. Phenomenological, we found that a power-law

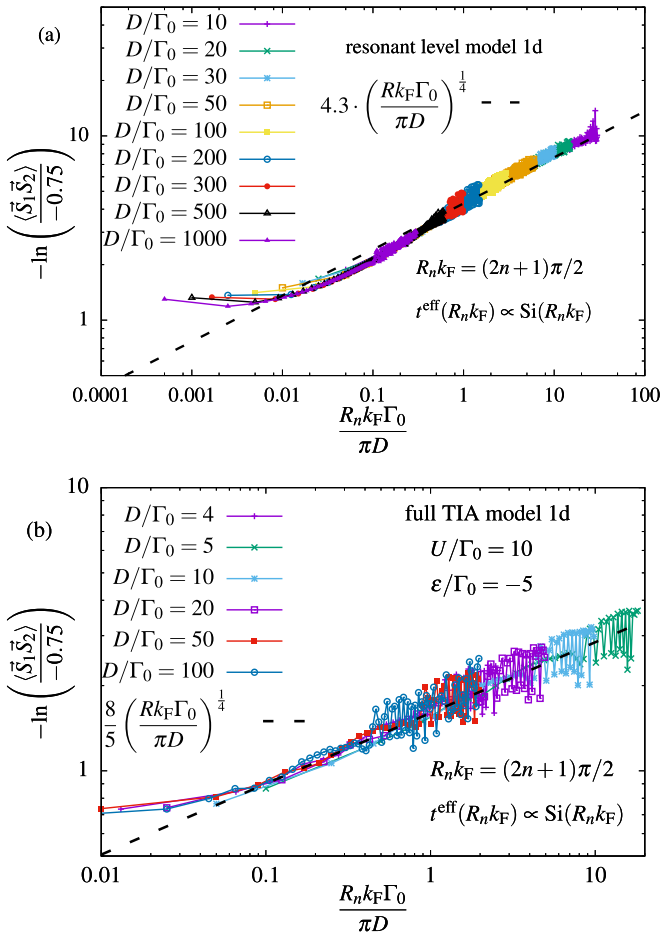

FIG. 8. Impurity spin-spin correlation as a function of $x = (R_n k_F \Gamma_0)/(\pi D)$ with $R_n k_F = (2n+1)\pi/2$. (a) Correlation function for the resonant level model ($U = 0$) calculated using Eq. (54) for a 1d linear dispersion. (b) Correlation function for TIAM with $U/\Gamma_0 = 10$, $\varepsilon/\Gamma_0 = -5$ calculated using the NRG with $N_s = 4000$ and $\Lambda = 3$.

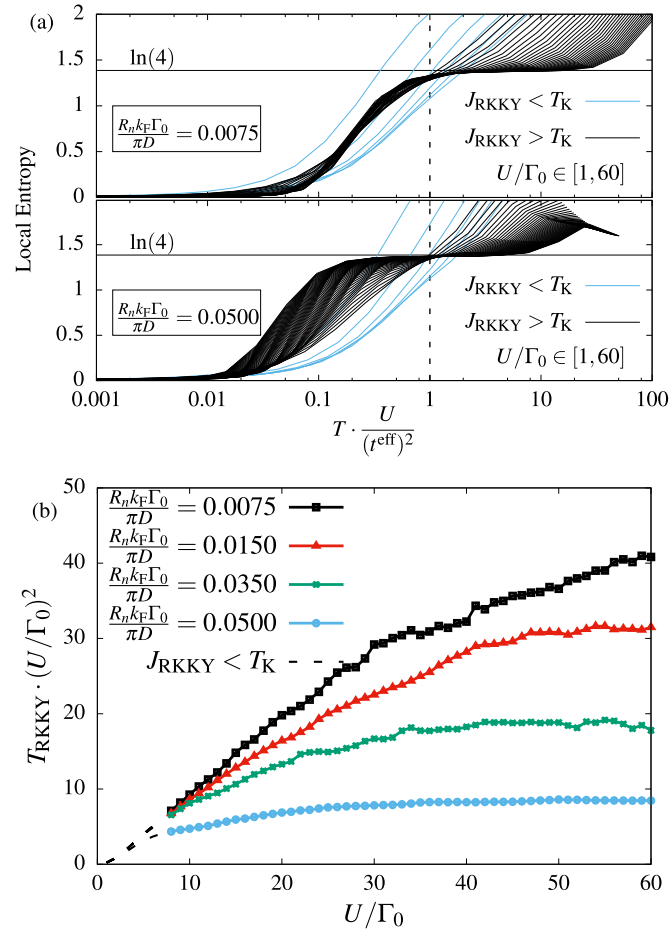

FIG. 9. (a) Local entropy of the impurities as a function of the dimensionless temperature $t = TU/t_{\rm eff}^2$ for two different effective distances $R_n k_F \Gamma_0/D$. The different lines represent different coupling strengths U/Γ_0 in a range of $1 < U/\Gamma_0 < 60$. The crossover temperature from the four-fold degenerate local moment regime a singlet with entropy ln(1) determines the energy scale $T_{\rm RKKY}$ of the RKKY interaction. (b) Energy scale $T_{\rm RKKY}$ rescaled by the square of the coupling U/Γ_0 as a function of the coupling in 1d. The different lines indicate different values for $\frac{d}{d\omega}\Gamma_\mu^-(\omega)|_{\omega=0} \propto \frac{R_n k_F \Gamma_0}{\pi D}$, which quantify the applicability of the effective Hamiltonian. NRG parameters: $N_s = 4000$ and $\Lambda = 3$.

fit $\propto x^{1/4}$ agrees remarkably with the data. Since the effective tunneling is nearly constant, only the corrections lead to a decay, wherefore the correlation is a universal function of the parameter that characterizes the strength of these corrections.

2. *U dependency of the RKKY interaction*

For $\frac{d}{d\omega}\Gamma_\mu^-(\omega)|_{\omega=0} \ll 1$, the corrections at large distances are small, and $H_{\rm TIAM} = H_{\rm TIAM}^+ + H_{\rm imp}^{\rm eff}$ is a good approximation. Our analysis, $J_{\rm RKKY}^{\rm AF} \propto [t^{\rm eff}]^2/U$, demonstrates that the RKKY interaction should be proportional to $1/U$ instead of the $1/U^2$ dependency expected by a separate two step transformation: (i) a Schrieffer Wolff transformation onto the two-impurity Kondo model and (ii) the perturbative calculation of $J_{\rm RKKY}$ using this two-impurity Kondo model.

Figure 9(a) depicts the local entropy of the impurities for a 1d linear dispersion, plotted against the dimensionless temperature $t = T \cdot U/(t^{\rm eff})^2$ for the distances R_n as defined above but a fixed ratio $R_n k_F \Gamma_0/D$ so that always an AF RKKY interaction is generated. The different lines represent different coupling strengths U/Γ_0 in a range of $1 < U/\Gamma_0 < 60$. The FP spectra of the NRG level flow distinguishes the two regimes $J_{\rm RKKY} > T_K$ (black line) and $J_{\rm RKKY} < T_K$ (blue lines). In the upper panel of Fig. 9(a), the corrections can be neglected, $Rk_F\Gamma_0/D\pi = 0.0075$, and the universal crossover of the entropy proves that $J_{\rm RKKY} \propto (t^{\rm eff})^2/U$.

This simple scaling does not hold for a larger $Rk_F\Gamma_0/D\pi = 0.05$ as demonstrated in the lower panel of Fig. 9(a). Since the crossover to a local singlet should still occur at a temperature scale $J_{\rm RKKY}$ the energy curves suggest a modification from the $1/U$ behavior.

In order to shed some light on the U dependency of $J_{\rm RKKY}$, we calculated the crossover temperature $T_{\rm RKKY}$ as a function of U/Γ_0. $T_{\rm RKKY}$ is defined as the temperature where the entropy $S_{\rm imp}$ has reached the value $S_{\rm imp}(T_{\rm RKKY}) = \frac{1}{2}\ln(4) = \ln(2)$. Figure 9(b) shows $T_{\rm RKKY} \cdot (U\Gamma_0)^2$ as a function of the coupling strength U/Γ_0 for different values of $\frac{R_n k_F \Gamma_0}{\pi D}$.

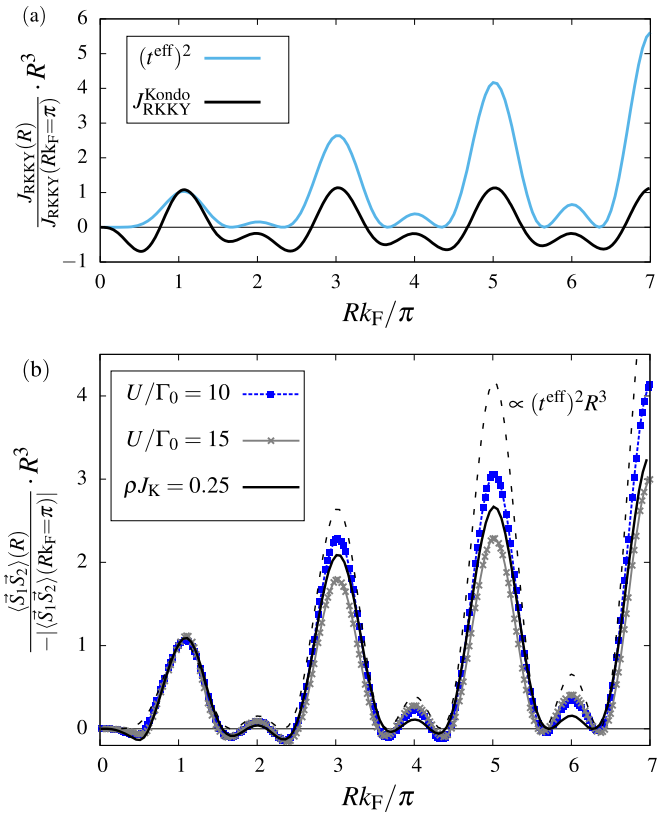

FIG. 10. (a) Comparison of the standard RKKY interaction for the TIKM and the square of the effective tunneling as a function of the distance for a 3d linear dispersion. (b) Impurity spin-spin correlation for the TIKM (black solid line) and the TIAM (lines with points) as a function of the distance for a 3d linear dispersion. Parameters: $D/\Gamma_0 = 10$, $N_s = 4000$, and $\Lambda = 2$.

The linear increase of the curves for small U proves the $1/U$ dependency. For very large U, the curves approach a constant. In this regime, $J_{\rm RKKY} \propto 1/U^2$ in accordance with the Schrieffer-Wolff transformation onto the TIKM. The crossover from a charge fluctuation driven $J_{\rm RKKY} \propto 1/U$ to a Kondo interaction driven $J_{\rm RKKY} \propto J^2 \propto 1/U^2$ does not only depend on U but is also strongly influenced by the ratio $Rk_{\rm F}\Gamma_0/D\pi$. Consequently, the replacement of the TIAM by the TIKM is distance-dependent and requires more care than just investigating the local regimes.

In the case of a linear dispersion in 3d, the corrections (61) are R independent and the amplitude of $t^{\rm eff}$ always decays as a function of R. Figure 10(a) shows a comparison of $J^{\rm Kondo}_{\rm RKKY}$ calculated by the textbook expression, which can be found in Appendix A of Ref. [59] as a black line with $(t^{\rm eff})^2$ as light blue line. While the envelope function of $J^{\rm Kondo}_{\rm RKKY}$ decays as R^{-3} as expected from the analytical formula, $(t^{\rm eff})^2 \times R^3$ is increasing with distance for small R. Consequently, $J^{\rm AF}_{\rm RKKY} \propto (t^{\rm eff})^2$ decays as R^{-2} in the wide-band limit for $U/D \ll 1$ in contrary to the expected R dependency of $J^{\rm Kondo}_{\rm RKKY}$.

While $J_{\rm RKKY}$ describes an effective spin-spin interaction in an effective local moment Hamiltonian, the R dependency of the spin-spin correlation function is a different property that is governed by the competition between the Kondo screening and the RKKY interaction. Figure 10(b) depicts $\langle \vec{S}_1\vec{S}_2\rangle R^3$ in the TIAM for moderate values of U/Γ_0 (blue and grey curve with points). For a better comparison of the decay of the envelope function, we normalized $\langle \vec{S}_1\vec{S}_2\rangle(R)$ at $Rk_{\rm F} = \pi$, where the correlations are AF, thus positive values belong to AF correlations.

The R dependence of $t^{\rm eff}$ governs the physics in the wide-band limit and for small U/Γ_0 [dashed line in Fig. 10(b)]. For $U \to 0$, the analytic equation (54) proves that the spin-spin correlation function is purely AF, whereas the sign of $J^{\rm Kondo}_{\rm RKKY}$ always oscillates with the distance. With increasing U/Γ_0, the FM correlations emerge continuously from the purely AF function and the power-law decay of the correlation function seems to cross from those of $(t^{\rm eff})^2$ over to those of $J^{\rm Kondo}_{\rm RKKY}$ for $U/\Gamma_0 \to \infty$. Note that we can not resolve this weak-coupling regime using the NRG, since the numerical noise is rapidly amplified by the R^3 scaling for $U/\Gamma_0 > 15$. We added $\langle \vec{S}_1\vec{S}_2\rangle$ calculated for the two-impurity Kondo model with a Kondo coupling $\rho J_{\rm K} = 0.25$ as a solid black line in Fig. 10(b). Just like small U/Γ_0 in the Anderson model, large Kondo couplings such as $\rho J_{\rm K} = 0.25$ lead to a suppression of the FM correlations due to the Kondo effect [70] and a slower decay as $J^{\rm Kondo}_{\rm RKKY}$, at least in the small distance regime.

V. SIMPLE CUBIC LATTICE

The RKKY interaction has been investigated for more than 60 years and it is well established, that the anisotropy caused by the lattice of the host has a strong influence on the RKKY interaction [71–76]. However, for a large Kondo-coupling $J_{\rm K}$ and small U/Γ_0 respectively, the Kondo effect has a strong influence on the spin-spin correlation function and the textbook expression for the RKKY interaction is not sufficient to describe the magnetic order [70]. Therefore the effective tunneling for an nonspherical band dispersion $\varepsilon_{\vec{k}}$ provides additional insight to established knowledge on the RKKY interaction.

In this section, we exemplify this by focusing on the well studied simple cubic lattice with lattice spacing a at half band filling. The dispersion $\epsilon_{\vec{k}}$ in d dimensions takes the form

$$\epsilon_{\vec{k}} = -\frac{D}{d}\sum_{\alpha=1}^{d}\cos(k_\alpha a), \tag{62}$$

for a nearest-neighbor tight-binding model with the hopping parameter $t = D/2d$.

Defining a nesting wave vector $\vec{Q}$ and the reciprocal lattice vectors $\vec{G}_\alpha$,

$$\vec{Q} = \frac{\pi}{a}\sum_{\alpha=1}^{d}\vec{e}_\alpha, \quad \vec{G}_\alpha = \frac{2\pi}{a}\vec{e}_\alpha, \tag{63}$$

which satisfy the relations $\epsilon_{\vec{k}\pm\vec{Q}} = -\epsilon_{\vec{k}}$ and $\epsilon_{\vec{k}\pm\vec{G}_\alpha} = \epsilon_{\vec{k}}$, we can always find a bijection $f : 1.\mathrm{Bz.} \to 1.\mathrm{Bz.}$, $\vec{k} \to \vec{k}'$, for which $\epsilon_{\vec{k}'} = -\epsilon_{\vec{k}}$,

$$f(\vec{k}) = \vec{k}' = \vec{k} + \vec{Q} + \sum_{\alpha=1}^{d} z_{\vec{k},\alpha}\vec{G}_\alpha, \quad z_{\vec{k},\alpha} \in \{\pm 1, 0\}. \tag{64}$$

Using this mapping, we analyze the effective DOSs with respect to inversion symmetry in energy space as well as P-H

symmetry:

$$\Gamma_e(-\epsilon, \vec{R}) = \pi V^2 \sum_{\vec{k}'} \delta(\epsilon - \epsilon_{\vec{k}'}) \cos^2\{\vec{k}'\vec{R}/2 - \Phi/2\},$$

$$\Gamma_o(-\epsilon, \vec{R}) = \pi V^2 \sum_{\vec{k}'} \delta(\epsilon - \epsilon_{\vec{k}'}) \sin^2\{\vec{k}'\vec{R}/2 - \Phi/2\}. \quad (65)$$

Due to the additional phase $\Phi/2$,

$$\Phi = \left(\vec{Q} + \sum_{\alpha=1}^{d} z_{\vec{k},\alpha}\vec{G}_\alpha\right)\vec{R}, \quad (66)$$

the hybridization function is P-H symmetric ($\Phi = n\pi$) for $R_\alpha/a \in \mathbb{Z}$ only. We can distinguish between the two different types of symmetries in the following way [51]:

$$\sum_{\alpha=1}^{d} R_\alpha = 2na \quad \longrightarrow \quad \text{first type}, \quad (67)$$

$$\sum_{\alpha=1}^{d} R_\alpha = (2n+1)a \quad \longrightarrow \quad \text{second type}. \quad (68)$$

Since the two types of P-H symmetry generate a contribution to the RKKY interaction with opposite sign, this result is equivalent to the general RKKY oscillations on a bipartite lattice at half-filling [77]. Moreover, the effective tunneling vanishes for impurities placed on the same sublattice.

A. Two-dimensional lattice at half-filling

Figure 11(a) shows the square of the effective hopping element in two dimensions, color-coded as a function of the impurity distance $\vec{R} = (R_x, R_y)$. The periodic structure in the two-dimensional plane indicate the importance of well-defined momenta in k-space that govern the RKKY interaction in real space.

In order to gain an analytical insight of the anisotropic structure, we rewrite the effective tunneling of Eq. (42) as a sum over the Brillouin zone

$$t^{\text{eff}}(\vec{R}) = \gamma \; s_\mu \sum_{\vec{k}\notin \text{FS}} \frac{1 + s_\mu \cos(\vec{k}\vec{R})}{\epsilon_{\vec{k}}}, \quad (69)$$

excluding the Fermi surface (FS) which does not contribute to the principle value integral. All distance independent constants are merged into the constant γ. The Fermi surface is given by a square with the corners located at $\vec{p}_{1/2} = \pm(0, \pi/a)$ and $\vec{l}_{1/2} = \pm(\pi/a, 0)$. Furthermore, we introduce the four midpoints of each side of the square, $M_{s,s'} = (s\pi/2a, s'\pi/2a)$ with $s, s' = \pm 1$.

In a second step, we perform a Fourier transformation into k space,

$$t^{\text{eff}}(\vec{q}) = \gamma \int d^2R \sum_{\vec{k}\notin \text{FS}} \frac{e^{i\vec{q}\vec{R}} \cos(\vec{k}\vec{R})}{\epsilon_{\vec{k}}}$$

$$= \begin{cases} \frac{\tilde{\gamma}}{\epsilon_{\vec{q}}}, & \vec{q} \notin \text{FS} \\ 0, & \vec{q} \in \text{FS} \end{cases} \quad (70)$$

exploiting the fact that the distance independent part vanishes by symmetry for a P-H symmetric conduction band. For

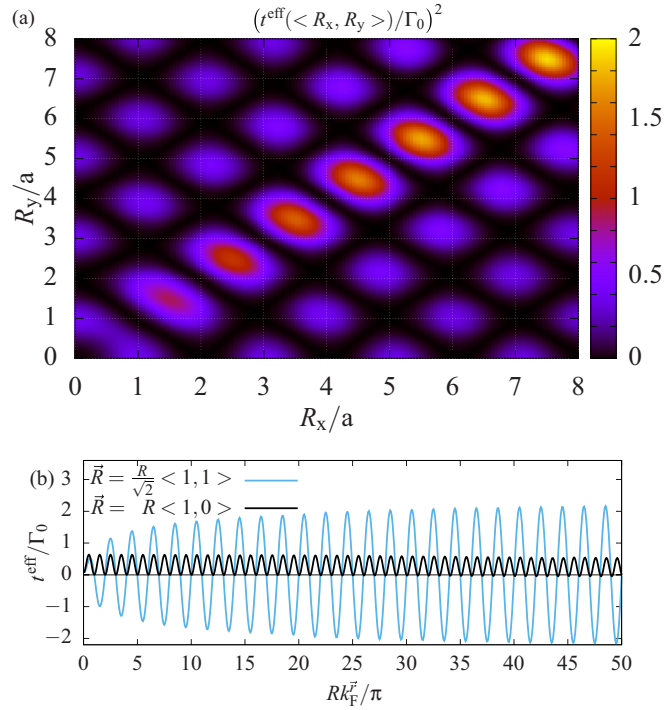

FIG. 11. (a) Square of the effective hopping element in two dimensions color-coded as a function of the impurity distance $\vec{R} = (R_x, R_y)$. The intersections of the grid correspond to the positions of the host atoms. (b) Effective tunneling along the basis and the diagonal direction. The absolute value of the distance is rescaled by $k_F^{\vec{r}}a/\pi = 1/2$ along the basis vector direction and $k_F^{\vec{r}}a/\pi = \sqrt{2}/2$ along the diagonal direction.

inversion symmetric dispersion, $\varepsilon_{\vec{k}} = \varepsilon_{-\vec{k}}$, $t^{\text{eff}}(\vec{q})$ obeys the relation

$$t^{\text{eff}}(\vec{q}) = t^{\text{eff}}(-\vec{q}) \quad (71)$$

and for P-H symmetry of the conduction band, the condition

$$t^{\text{eff}}(\vec{R} = 0) = \int_{-\infty}^{\infty} t^{\text{eff}}(\vec{q}) d\vec{q} = 0 \quad (72)$$

must hold.

The largest contribution to the k summation in Eq. (70) is generated at the corners of FS, located at $\vec{p}_{1/2} = \pm(0, \pi/a)$ and $\vec{l}_{1/2} = \pm(\pi/a, 0)$, and we can approximate the Fourier transformation $t^{\text{eff}}(\vec{q})$ by a sum of δ functions,

$$t^{\text{eff}}_{\text{corner}}(\vec{q}) \propto \sum_{i\in\{1,2\}} [\delta(\vec{q} + \vec{p}_i) - \delta(\vec{q} + \vec{l}_i)], \quad (73)$$

with an appropriate prefactor that is independent of $\vec{q}$.

This simplified expression can be transformed back into real space. Along the direction $\vec{n} = \vec{R}/R$, $R = |\vec{R}|$, $t^{\text{eff}}_{\text{corner}}(\vec{R})$ is given by a product of modulations,

$$t^{\text{eff}}_{\text{corner}}(\vec{R}) \propto \sin\left(Rk^{\vec{r}}_{\text{F},+}\right) \sin\left(Rk^{\vec{r}}_{\text{F},-}\right), \quad (74)$$

governed by the two characteristic spatial frequencies

$$k^{\vec{r}}_{\text{F},\pm} = \frac{\pi}{2a}|n_x \pm n_y|. \quad (75)$$

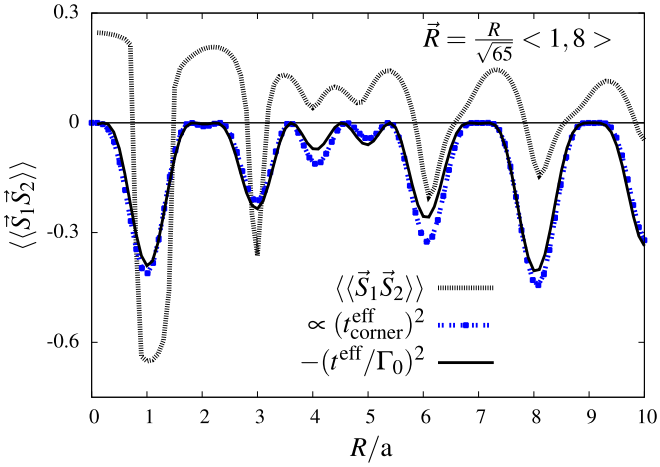

FIG. 12. Impurity spin-spin correlation function in comparison with the full effective tunneling $t^{\rm eff}$ and the contributions that originate from the corners $\vec{p}_{1,2}, \vec{l}_{1,2}$ $t^{\rm eff}_{\rm corner}$ along the direction $\vec{r} = \frac{1}{\sqrt{65}}(\vec{e}_1 + 8\vec{e}_2)$ with $D/\Gamma_0 = 10$ and $U/\Gamma_0 = 30$. NRG parameters: $N_s = 3000$ and $\Lambda = 4$.

Along the basis vector direction $\vec{n} = \vec{e}_\alpha$, the frequencies are identical and the sign of the effective tunneling remains positive.

Within this approximation, the amplitude of the oscillating effective hopping remains constant. This provides a better understanding why the full $t^{\rm eff}(\vec{R})$ plotted in Fig. 11(b) does not decay as a function of the distance R and explains the different oscillation frequencies in the different spatial directions.

To illustrate the quality of the approximation, a comparison between the full $t^{\rm eff}(\vec{R})$ and the approximative quantity $t^{\rm eff}_{\rm corner}(\vec{R})$ obtained from Eq. (74) is shown for a more generic direction $\vec{n} = \frac{1}{\sqrt{65}}(\vec{e}_1 + 8\vec{e}_2)$ in Fig. 12. The plot demonstrates that the oscillations of the AF contribution to the RKKY interaction are determined by $k^{\vec{r}}_{{\rm F},\pm}$. We also added the spatial dependency of the impurity spin-spin correlation function along the same direction as grey dotted curve to Fig. 12 illustrating that the sign changes and the oscillatory behavior tracks the spatial dependency of $t^{\rm eff}$.

Since $k^{\vec{r}}_{{\rm F},-}$, and with that Eq. (74), vanishes along the diagonal $r_x = r_y$, the AF contributions cannot originate from the points $\vec{p}_{1/2}$ and $\vec{l}_{1/2}$ in that case. Therefore we reexamine the original expression. The main contributions to the sum in Eq. (69) stem from k-points around the Fermi surface

$$\vec{k}'_\pm = \lim_{\delta\to 0} \vec{k}_{\in {\rm FS}} \pm \delta \vec{n}^{\rm FS}_{\vec{k}}, \tag{76}$$

where $\vec{n}^{\rm FS}_{\vec{k}}$ denotes the local normal vector of the FS. If the oscillations of the numerator $\cos(\vec{k}\vec{R})$ in the vicinity of the FS are small, in general for short distances, the generic spatial structure should be reproduced by focusing on the summation of a very small k-shell around the FS and we obtain the approximation

$$t^{\rm eff}(\vec{R}) \approx \tilde{t}^{\rm eff}(\vec{R}) \propto \sum_{\vec{k}'_+} \frac{\cos(\vec{k}'_+ \vec{R})}{\epsilon_{\vec{k}'_+}} + \sum_{\vec{k}'_-} \frac{\cos(\vec{k}'_- \vec{R})}{\epsilon_{\vec{k}'_-}}. \tag{77}$$

substituting $\epsilon_{\vec{k}'_\pm} = \pm\delta \nabla_{\vec{n}^{\rm FS}_{\vec{k}}} \epsilon_{\vec{k}}$ into this expression, we can restrict Eq. (77) to a summation over the Fermi surface and a directional derivation along $\vec{n}^{\rm FS}_{\vec{k}}$:

$$\begin{aligned}\tilde{t}^{\rm eff}(\vec{R}) &\propto \sum_{\vec{k}\in {\rm FS}} \lim_{\delta\to 0} \frac{\cos\left((\vec{k} + \delta\vec{n}^{\rm FS}_{\vec{k}})\vec{R}\right) - \cos\left((\vec{k} - \delta\vec{n}^{\rm FS}_{\vec{k}})\vec{R}\right)}{\delta \nabla_{\vec{n}^{\rm FS}_{\vec{k}}} \epsilon_{\vec{k}}} \\ &= \sum_{\vec{k}\in {\rm FS}} \frac{\nabla_{\vec{n}^{\rm FS}_{\vec{k}}} \cos(\vec{k}\vec{R})}{\nabla_{\vec{n}^{\rm FS}_{\vec{k}}} \epsilon_{\vec{k}}}.\end{aligned} \tag{78}$$

We have shown above that the corners of the 2d Fermi surface of a simple cubic lattice, at which the nominator and denominator in Eq. (78) vanishes, do not contribute to $t^{\rm eff}(\vec{R})$ along the diagonal in real space. Therefore we focus on the four midpoints $M_{s,s'} = (s\pi/2a, s'\pi/2a)$. The dispersion is linear around these points close to the FS and $\nabla_{\vec{n}^{\rm FS}_{\vec{k}}} \epsilon_{\vec{k}} \approx 2$ in appropriate units. Therefore we replace the denominator in (78) by a constant and integrate over some part of the FS around these midpoints, which can be easily parameterized by a 1d integral,

$$\begin{aligned}\tilde{t}^{\rm eff}_{\rm mid}(\vec{R}) \propto &\left(\int_{\frac{\pi}{2a}-\tau}^{\frac{\pi}{2a}+\tau} dk_x + \int_{-\frac{\pi}{2a}-\tau}^{-\frac{\pi}{2a}+\tau} dk_x\right) \\ &\left[\left(\vec{n}^{\rm FS}_{k_x}\vec{R}\right) \sin\left\{(R_x k_x - R_y|k_x|) + R_y \frac{\pi}{a}\right\}\right].\end{aligned} \tag{79}$$

The distance from the midpoints included here is parametrized by τ, and the explicit shape of the FS, $|k_y| = \pi/a - |k_x|$, was inserted.

For a general direction, this leads to small contributions due to the oscillations of the integrand. Only along the diagonal direction, these oscillations cancel. In addition $R_y\pi/a = Rk^{\vec{r}}_{{\rm F},+}$ holds and we find a linear increase with the distance R,

$$\tilde{t}^{\rm eff}_{\rm mid}\left(\frac{R}{\sqrt{2}}\begin{pmatrix}1\\1\end{pmatrix}\right) \propto R\, \sin\left(Rk^{\vec{r}}_{{\rm F},+}\right). \tag{80}$$

This provides the deeper understanding of the surprising increase of the amplitude of the full $t^{\rm eff}(\vec{R})$ shown in Fig. 11(b). Our analytical calculation links this observation to the properties of the dispersion at the midpoints of the FS for the P-H symmetric band. Note that for large values of R, the oscillations around the FS in the nominator of Eq. (77) lead to a damping of the linear increase: the simplification entering Eq. (78) are not valid for large R.

For larger distances R, the amplitude of the tunneling stays constant in all directions as a consequence of the perfect FS-nesting for a 2d simple-cubic dispersion at half-filling. The linear increase of the effective tunneling along the diagonal direction strongly depends on the structure of the FS, but is not a consequence of FS-nesting and the divergence of the Lindhard function in momentum space, respectively.

The spatial and band width corrections to the spin correlation function discussed in Sec. IV C predict a decay of the correlation function even for constant $t^{\rm eff}$ that contains the exact AFM RKKY interaction in the limit $\Gamma_0/D \to 0$. Figure 13 depicts the impurity spin-spin correlation as a function of the distance along the basis and the diagonal

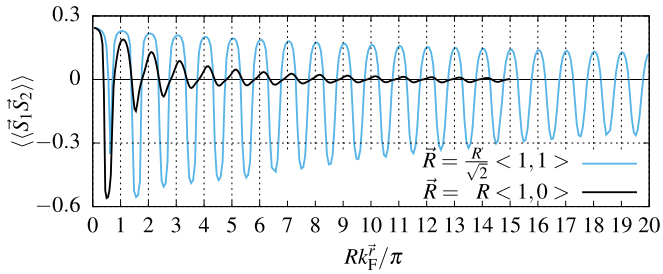

FIG. 13. NRG calculations of the impurity spin-spin correlation function along the basis vector and the diagonal direction with $D/\Gamma_0 = 10$ and $U/\Gamma_0 = 30$. NRG parameters: $N_s = 3000$ and $\Lambda = 4$.

direction. As expected from the initially linearly increasing and than constant t^{eff} in the diagonal direction, the correlation function dominates in this direction. Its amplitude only shows a slow decay as a function of R caused by the finite bandwidth.

B. Particle and hole doping in two dimensions

The strong influence of the explicit shape of the Fermi surface on the effective tunneling and the RKKY interaction, respectively, can be demonstrated by adding an additional chemical potential μ, which influences the energy dispersion of the host and the level energy of the impurities

$$\epsilon_{\vec{k}} \to \epsilon_{\vec{k}} + \mu\,; \quad \epsilon^f \to \epsilon^f + \mu. \tag{81}$$

Obviously, the chemical potential breaks P-H symmetry in the initial conduction band but preserves parity. Our analysis, however, remains valid and the P-H asymmetry can be still casted into an distance-dependent hopping term

$$\begin{aligned} t^{\text{eff}}(\vec{R}) &= \Re(\Delta_e^-(0,\vec{R})) - \Re(\Delta_o^-(0,\vec{R})) \\ &= \gamma \sum_{\vec{k}\notin \text{FS}} \frac{\cos(\vec{k}\vec{R})}{\epsilon_{\vec{k}}} \end{aligned} \tag{82}$$

In a 2d simple cubic lattice with a nearest-neighbor tight-binding description of the band dispersion, the sign of the chemical potential determines the topology of the FS; a negative value of μ leads to a spherical structure of the FS, whereas a positive potential induces general hole pockets.

In Sec. V A, we have shown that either the midpoints or the corner points of the square FS are responsible for the main contributions to the effective tunneling, depending on the directional alignment of the impurities. Since a very weak doping away from half-filling only deforms the FS around the corner points, we expect a strong influence on the effective tunneling only along the basis vector direction. Figure 14(a) depicts the color-coded effective tunneling for electron and hole doping, i.e., holelike and spherical FS. While the general structure along the diagonal direction matches the P-H symmetric case, the spatial frequency along the basis vector direction varies significantly.

To understand this change in the frequency in the direction of the basis vectors, we focus on $t_x^{\text{eff}}(R) = t^{\text{eff}}(R\vec{e}_x)$ and

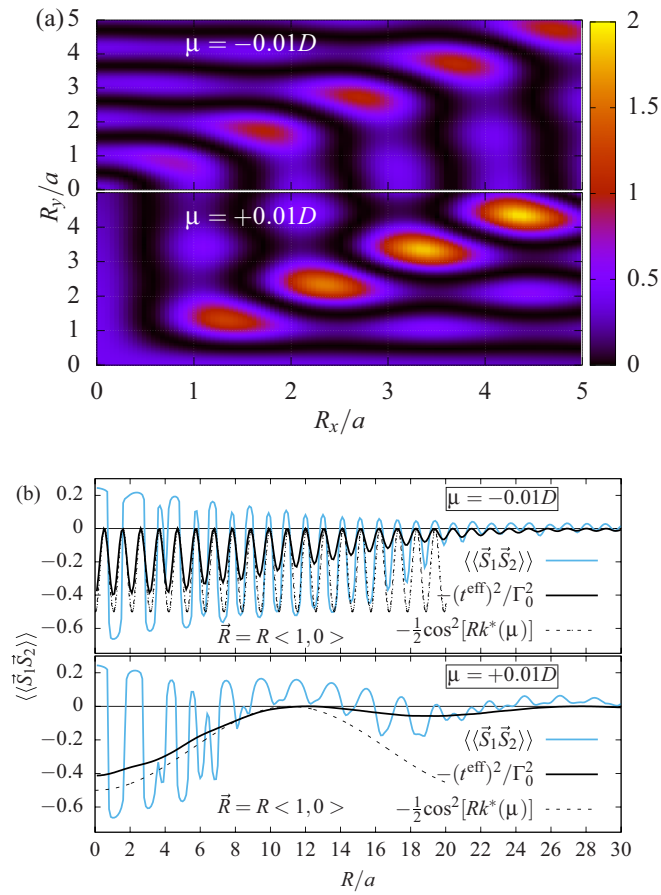

FIG. 14. (a) Square of the effective hopping element in 2d as a function of the impurity distance $\vec{R} =< R_x/a,\ R_y/a >$. The frequency along the basis vector directions strongly depends on the sign of the chemical potential and the topology of the FS, respectively. The intersections of the grid correspond to the positions of the host atoms. (b) NRG calculation of the impurity spin-spin correlation function (blue line) and the square of the effective tunneling (black line) along the basis vector direction. We added the analytically extracted spatial contribution $\cos^2(k_x^*(\mu)R)$ as a dashed line. Parameters: $D/\Gamma_0 = 10$, $U/\Gamma_0 = 30$, $N_s = 3000$, and $\Lambda = 4$.

perform a one-dimensional Fourier transformation of (69):

$$\begin{aligned} t^{\text{eff}}(q) &= \gamma \int_{-\infty}^{\infty} dR \sum_{\vec{k}\notin \text{FS}} \frac{e^{iqR}\cos(k_x R)}{\epsilon_{\vec{k}}} \\ &= \frac{\pi\gamma}{t} \sum_{\vec{k}\notin \text{FS}} \frac{\delta(q-k_x)+\delta(q+k_x)}{\cos(k_x a)+\cos(k_y a)+\mu/t}\,, \end{aligned} \tag{83}$$

where we substituted $\epsilon_{\vec{k}}$ defined with respect to the chemical potential.

We have to perform a k_y summation for every q while k_x is fixed by δ functions. $t^{\text{eff}}(q)$ has the largest contribution for those q values for which many k vectors $(\pm q, k_y)$ are very close to the FS.

We recall that upon hole doping the Fermi surface shrinks and becomes more spherical. While the midpoints remain almost unaltered, the major change occurs in the vicinity of the corner points, which are shifted to smaller k_x (k_y) values for $k_y = 0$ ($k_x = 0$). For negative μ, the major contribution

arises from the intersection of the FS with the k_x axis since the FS is perpendicular to the axis at theses shifted corner points. Solving $\epsilon_{k_y=0} = 0$ for $k_x^*(\mu)$ yields

$$k_x^*(\mu)a = \arccos(|\mu| - 1) \tag{84}$$

and therefore, the major contributions stem from large $k_x^*(\mu)$ that develop adiabatically from $k_x = \pi$. Simultaneously, the contributions from the second pair of corner points, $(0, \pm\pi/a)$, rapidly vanishes with increasing hole doping. At the end, we are left with

$$t^{\text{eff}}(q, \mu) \approx \delta(q + k_x^*(\mu)) + \delta(q - k_x^*(\mu)) \tag{85}$$

$$\Leftrightarrow \quad t^{\text{eff}}(R, \mu) \propto \cos[R k_x^*(\mu)]\,. \tag{86}$$

The missing contribution for $k_x = 0$ leads to a doubling of the spatial frequency away from half-filling as can be seen in Fig. 14(a) along the x (y) axis compared to Fig. 11(a).

The situation is qualitatively different for electron doping ($\mu > 0$), where the FS is formed by the four hole pockets. The FS does not intersect with either k axis. However, the FS becomes parallel to the k_y axis close to the Brillouin zone boundary for a small value $k_x^*(\mu)$,

$$k_x^*(\mu) = \arccos(1 - \mu)\,. \tag{87}$$

$k_x^*(\mu)$ evolves from $k_x = 0$ at half-filling, while the contribution from $k_x = \pi/a$ vanished rapidly with increasing μ. As a consequence, the spatial oscillation of $t^{\text{eff}}(\vec{R})$ along the x or y axis are very slow as shown in Fig. 14(a) for $\mu = 0.01D$.

A spherical deformation of the FS leads to a fast oscillation of the effective tunneling with $k_x^*(\mu) \approx 2 \cdot k_{\text{F},\pm}^{\vec{r}}$, in contrast to slow oscillations in the presence of hole pockets. This is illustrated for the two different cases in Fig. 14(b) where the full $t^{\text{eff}}(\vec{R})$ (black solid curve) is compared to the main contribution stemming from the spatial frequency $k_x^*(\mu)$ (dashed line).

We augment this analysis for $t^{\text{eff}}(\vec{R})$ with the NRG calculation of the impurity spin-spin correlation function along the basis vector direction, for positive and negative values of the chemical potential.

For a negative chemical potential and a spherical FS, the antiferromagnetic part of the correlation function almost shows the same oscillations as the square of the effective tunneling as can be seen in the upper panel of Fig. 14(b). The small deviations of the correlation function from the behavior of the effective tunneling can be ascribed to the FM part of the RKKY interaction which is not captured by the effective tunneling and evolves for finite U/Γ_0.

In the presence of hole pockets, lower panel of Fig. 14(b), the general characteristics of the slow oscillations can be identified in the impurity spin-spin correlation function, too. In the vicinity of a vanishing effective tunneling, only ferromagnetic correlations are observed. The sign of the correlation function oscillates only in the presence of an antiferromagnetic contribution to the RKKY interaction, generated by $t^{\text{eff}}(\vec{R})$.

Figure 15 shows the spin-spin correlation function (blue curve) as well as the $[t^{\text{eff}}]^2$ (black curve) as a function of μ for a constant impurity distance $\vec{R}$ in order to illustrate the nonlinear dependence of the frequency of the spin-spin correlation function on the chemical potential.

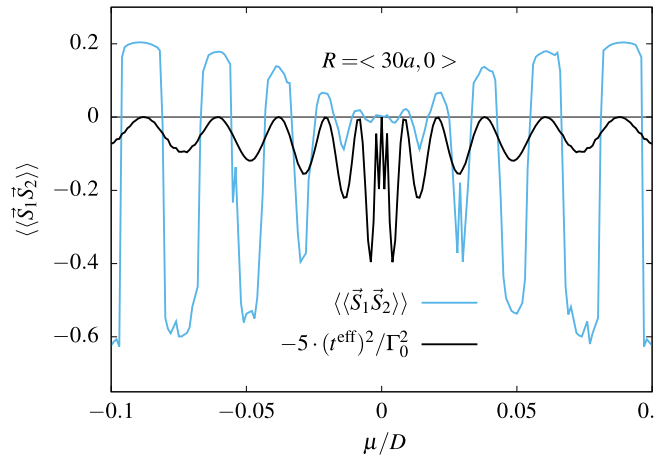

FIG. 15. NRG calculation of the impurity spin-spin correlation function for a coupling of $U/\Gamma_0 = 30$ and the square of the effective tunneling, plotted against the dimensionless chemical potential. The RKKY interaction oscillates as a function of μ/D. Parameters: $D/\Gamma_0 = 10$, $U/\Gamma_0 = 30$, $\text{N}_\text{s} = 3000$, and $\Lambda = 4$.

C. Three-dimensional lattice at half-filling

In the previous sections, we demonstrated that the richer spatial dependency of the spin-spin correlation function as well as the effective tunneling, beyond the simplified isotropic $2k_F$ oscillations, originates from the generically nonspherical FS and can be analyzed by the investigation of the analytical properties of the integrals.

We now extend our study to the 3d simple cubic dispersion. The effective tunneling term along the three symmetry directions is depicted in Fig. 16. Just like in two dimensions, the superposition of different frequencies account for complex oscillations. The symmetry properties on the lattice places, defined by Eqs. (67) and (68), are fulfilled.

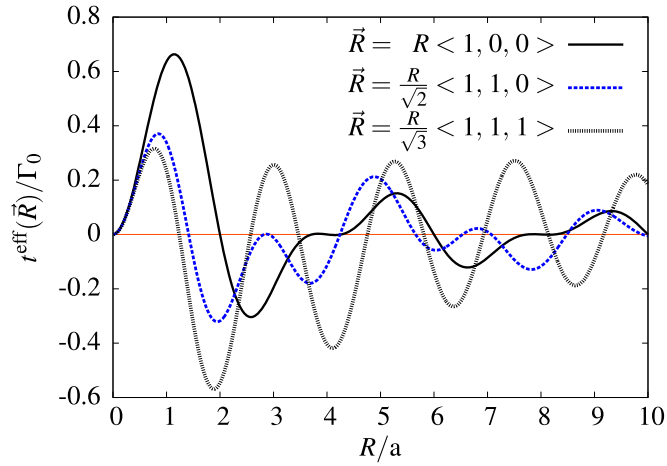

FIG. 16. Effective hopping element in 3d plotted against the dimensionless impurity distance R/a. The anisotropic lattice structure is mirrored in a strong dependence of the spatial frequency on the directionality.

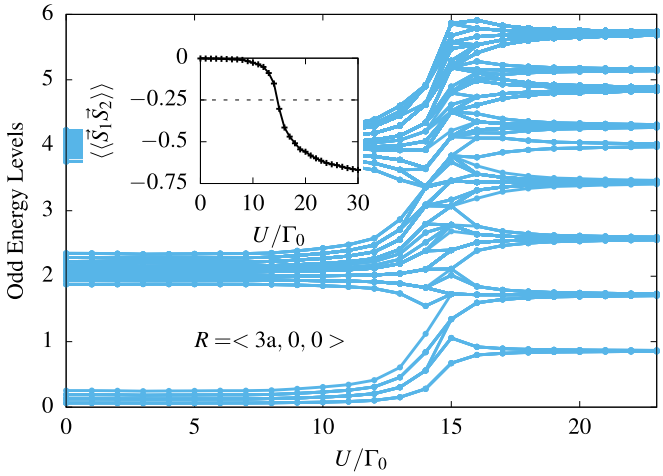

FIG. 17. Doniach scenario in the TIAM for an impurity distance $\vec{R} = \langle 3a, 0, 0\rangle$. The inset depicts the impurity spin-spin correlation function and illustrates the interimpurity singlet formation for large values of U/Γ_0. The continuous energy flow between the two fixed points displays a crossover. NRG parameters: $N_s = 3000$ and $\Lambda = 4$.

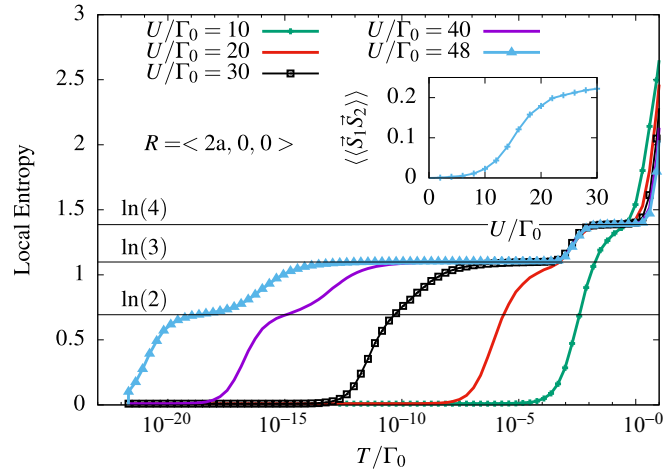

FIG. 18. The impurity entropy vs T for different values of U for an impurity distance $\vec{R} = \langle 2a, 0, 0\rangle$. (Inset) Impurity spin-spin correlation function. NRG parameters: $N_s = 3000$, and $\Lambda = 4$.

1. AFM RKKY coupling: the Doniach scenario

In Sec. III, we discussed the transition from the Kondo singlet to an interimpurity singlet ground state as a function of an additional magnetic exchange interaction J_{12} in the Hamiltonian. In principle, the transition can also be realized by changing the ratio between the antiferromagnetic RKKY interaction and the Kondo temperature. The transition is typically discussed in terms of the Kondo coupling J_K in the context of the TIKM. In lattice systems this is referred to as the Doniach scenario [40]: the heavy Fermi liquid [39] is replaced at the QCP by an AF ordered state generated by the interimpurity singlets in a lattice.

Decreasing J_K causes an exponential decay of T_K, whereas the RKKY interaction only falls off as J_K^2 leading to an increase of the ratio J_{RKKY}/T_K. In the TIAM, the Kondo coupling J_K is related to the ratio of the Coulomb interaction U and the coupling strength Γ_0.

Linneweber *et al.* investigated the TIAM on the three-dimensional simple cubic lattice via a Gutzwiller variational approach and found such a QCP at a critical U_c provided the impurities are placed on the lattice sites [78]. The authors indicated that their QCP is probably an artifact of the Gutzwiller variational approach: the Gutzwiller trial wave function only includes local correlations on the impurity site while the NRG reveals already for the Kondo problem the extended nature of the correlated singlet [59,60].

If the impurities are placed on different sublattices, e.g., if they are separated by an odd number of the lattice spacing along the basis vector direction $\vec{R} = R^{odd}\langle 1, 0, 0\rangle$, the RKKY interaction is always antiferromagnetic. The NRG level flow of the stable FP as a function of U/Γ_0 is shown in Fig. 17. Clearly, the FP changes continuously from the SC fixed point with P-H symmetry breaking scattering term to the interimpurity singlet FP with the absence of a phase shift of the conduction electron states. The crossover occurs in the vicinity of $U/\Gamma_0 \approx 14$. The inset of Fig. 17 depicts the corresponding impurity spin-spin correlation and illustrated the formation of a local interimpurity singlet in the limit of $U/\Gamma_0 \to \infty$. No indication of a QCP is found by the NRG when increasing U.

The absence of the QCP originates from the fact, that the RKKY interaction cannot only be reduced to a spin exchange interaction. The RKKY driven charge exchange between the impurities, which is responsible for the antiferromagnetic interaction, generates marginal relevant operators in the renormalization flow, driving the system away from the QCP. In order to restore the QCP as a function of U/Γ_0, a compensating effective tunneling $-t^{eff}(\vec{R})$ has to be added as well as an additional, antiferromagnetic spin exchange J_{12} that would control the distance to the Varma-Jones type QCP.

2. FM RKKY coupling

If the impurities are placed on the same sublattice, the RKKY interaction is ferromagnetic according to Eq. (67). After the local moments are formed, they align with increasing RKKY interaction, and the resulting triplet state is screened in a two-stage Kondo effect [21]. This is clearly visible by tracking the impurity entropy as a function of temperature [27] for different values of U as depicted in Fig. 18. The local moment formation occurs on a scale of U/Γ_0 leading to a ln(4) impurity entropy contribution at intermediate temperatures. By lowering T further, we observe the crossover to a local triplet on the scale defined by J_{RKKY}: The larger U is, the more pronounced the consecutive two stage Kondo screening is visible revealing the different unstable FP of the RG flow.

The inset of Fig. 18 shows the impurity spin-spin correlation as a function of U/Γ_0 and displays the formation of a local interimpurity triplet. Since the Kondo temperature is suppressed with increasing U, the RKKY interaction dominates at higher temperature and favors a correlated triplet that is collectively screened in a two stage process for $T \to 0$.

We do not find a breakdown of the Kondo effect in the presence of FM RKKY interaction found in a recent perturbative RG treatment of the TIKM [42]. While this RG approach focuses on the renormalization of the effective Kondo coupling

at one of the impurity sites, the NRG includes all couplings for both impurities on equal footing.

VI. SUMMARY AND CONCLUSION

Mapping the TIAM onto degrees of freedom with even and odd parity symmetry generates two, in general P-H asymmetric, hybridization functions. Both hybridization functions can be decomposed into a symmetric part with respect to the frequency and an asymmetric correction. Neglecting the asymmetric part generates always a FM RKKY interaction. A QCP as observed by Varma and Jones is found after adding a direct antiferromagnetic exchange interaction. The asymmetric part, however, is responsible for an additional relevant scattering term at zero energy and hence destroys the Varma and Jones QCP.

We have shown that the effect of the asymmetric part is equivalent to an effective tunneling term between the two impurities: replacing the full hybridization function by the symmetrized contribution and this local tunneling term leads to the identical low-temperature FP spectrum in the NRG.

This opened the door for restoring the QCP by adding a suitable tunneling term to the full Hamiltonian at a fixed distance R or by adjusting the distance between the impurities. While the counter term can be analytically calculated for P-H symmetric impurities, the term is determined by a numerical iteration procedure for P-H asymmetric impurities. Using the estimates from the case of P-H symmetric impurities as the initial value, the parameter t^{eff} or R is iteratively adjusted such that the lowest single-particle excitations in the even and the odd channel are equal. We checked that these results are consistent with the scattering phases of both single-particle Green functions and found that both phases are also identical at the QCP.

Using the replacement of the full model by a symmetric hybridization function and a local tunneling term, provides a better understanding of the antiferromagnetic contribution to the RKKY interaction. In contrary to the RKKY interaction of a two-impurity Kondo model resulting from a Schrieffer-Wolff transformation, we find $J^{\mathrm{AF}}_{\mathrm{RKKY}} \propto (t^{\mathrm{eff}})^2/U$. Only for very large U, a crossover to $J^{\mathrm{AF}}_{\mathrm{RKKY}} \propto 1/U^2$ is observed. Furthermore, the value of J_{RKKY} decays much more rapidly than $J^{\mathrm{AF}}_{\mathrm{RKKY}}$. The distance dependency of the corresponding spin-spin correlations, however, tracks the distance dependency of $(t^{\mathrm{eff}})^2$ indicating a significant deviation for small and intermediate U.

For a constant tunneling t^{eff}, the impurity spin-spin correlation function is governed by a dimensionless variable that accounts for the distance-dependent correction and the correction to the wide-band limit.

We analyzed the spatial anisotropy of the RKKY interaction as well as the impurity spin-spin correlation function for square lattices in different dimensions. We identified the major spatial frequencies that govern the oscillation in real space for different chemical potentials close to half-filling and linked them to the single-particle dispersion as well as the shape of the Fermi surface.

No quantum phase transition is found upon increasing the local Coulomb repulsion for a distance at which the RKKY interaction is AF. The spin-spin correlation function as well as the NRG low-temperature FP spectrum changes continuously from the strong-coupling FP towards the flow characterizing the local singlet phase. For a distance leading to a FM RKKY interaction, a two-stage Kondo effect only becomes more pronounced with increasing U. Therefore the Doniach scenario for heavy fermion QCP requires lattice effects that are included in the particle-hole Bethe saltpeter equation that enters the lattice spin susceptibility.

ACKNOWLEDGMENTS

We acknowledge fruitful discussions with J. Bünemann, F. Gebhard, and H. Kroha. B.L. thanks the Japan Society for the Promotion of Science (JSPS) and the Alexander von Humboldt Foundation.

[1] D. Loss and D. P. DiVincenzo, Phys. Rev. A **57**, 120 (1998).
[2] G. Burkard, D. Loss, and D. P. DiVincenzo, Phys. Rev. B **59**, 2070 (1999).
[3] B. A. Trauzettel, D. V. Bulaev, D. Loss, and G. Burkard, Nat. Phys. **3**, 192 (2007).
[4] A. Greilich, D. R. Yakovlev, A. Shabaev, A. L. Efros, I. A. Yugova, R. Oulton, V. Stavarache, D. Reuter, A. Wieck, and M. Bayer, Science **313**, 341 (2006).
[5] M. M. Glazov, J. Appl. Phys. **113**, 136503 (2013).
[6] I. Žutić, J. Fabian, and S. Das Sarma, Rev. Mod. Phys. **76**, 323 (2004).
[7] M. Misiorny, M. Hell, and M. R. Wegewijs, Nat. Phys. **9**, 801 (2013).
[8] W. Han, R. K. Kawakami, M. Gmitra, and J. Fabian, Nat. Nano **9**, 794 (2014).
[9] H. Johll, M. D. K. Lee, S. P. N. Ng, H. C. Kang, and E. S. Tok, Sci. Rep. **4**, 7594 (2014).
[10] O. V. Yazyev and L. Helm, Phys. Rev. B **75**, 125408 (2007).
[11] J. Bork, Y.-h. Zhang, L. Diekhoner, L. Borda, P. Simon, J. Kroha, P. Wahl, and K. Kern, Nat. Phys. **7**, 901 (2011).
[12] T. Esat, B. Lechtenberg, T. Deilmann, C. Wagner, P. Kruger, R. Temirov, M. Rohlfing, F. B. Anders, and F. S. Tautz, Nat. Phys. **12**, 867 (2016).
[13] N. Atodiresei, J. Brede, P. Lazić, V. Caciuc, G. Hoffmann, R. Wiesendanger, and S. Blügel, Phys. Rev. Lett. **105**, 066601 (2010).
[14] L. Bogani and W. Wernsdorfer, Nat. Mater. **7**, 179 (2008).
[15] S. Sanvito, Chem. Soc. Rev. **40**, 3336 (2011).
[16] W. J. M. Naber, S. Faez, and W. G. van der Wiel, J. Phys. D **40**, R205 (2007).
[17] V. A. Dediu, L. E. Hueso, I. Bergenti, and C. Taliani, Nat. Mater. **8**, 707 (2009).
[18] A. J. Drew, J. Hoppler, L. Schulz, F. L. Pratt, P. Desai, P. Shakya, T. Kreouzis, W. P. Gillin, A. Suter, N. A. Morley, V. K. Malik, A. Dubroka, K. W. Kim, H. Bouyanfif, F. Bourqui,

C. Bernhard, R. Scheuermann, G. J. Nieuwenhuys, T. Prokscha, and E. Morenzoni, Nat. Mater. **8**, 109 (2009).
[19] A. Spinelli, M. Gerrits, R. Toskovic, B. Bryant, M. Ternes, and A. F. Otte, Nat. Commun. **6**, 10046 (2015).
[20] C. Jayaprakash, H. R. Krishna-murthy, and J. W. Wilkins, Phys. Rev. Lett. **47**, 737 (1981).
[21] B. A. Jones and C. M. Varma, Phys. Rev. Lett. **58**, 843 (1987).
[22] B. A. Jones, C. M. Varma, and J. W. Wilkins, Phys. Rev. Lett. **61**, 125 (1988).
[23] O. Sakai, Y. Shimizu, and T. Kasuya, Solid State Commun. **75**, 81 (1990).
[24] R. M. Fye, J. E. Hirsch, and D. J. Scalapino, Phys. Rev. B **35**, 4901 (1987).
[25] M. Vojta, R. Bulla, and W. Hofstetter, Phys. Rev. B **65**, 140405 (2002).
[26] O. Sakai, Y. Shimizu, and N. Kaneko, Physica B **186**, 323 (1993).
[27] A. Schwabe, M. Hänsel, M. Potthoff, and A. K. Mitchell, Phys. Rev. B **92**, 155104 (2015).
[28] F. W. Jayatilaka, M. R. Galpin, and D. E. Logan, Phys. Rev. B **84**, 115111 (2011).
[29] E. Sela, A. K. Mitchell, and L. Fritz, Phys. Rev. Lett. **106**, 147202 (2011).
[30] A. K. Mitchell, E. Sela, and D. E. Logan, Phys. Rev. Lett. **108**, 086405 (2012).
[31] A. Schwabe, D. Gütersloh, and M. Potthoff, Phys. Rev. Lett. **109**, 257202 (2012).
[32] I. Titvinidze, A. Schwabe, N. Rother, and M. Potthoff, Phys. Rev. B **86**, 075141 (2012).
[33] I. Titvinidze and M. Potthoff, J. Korean Phys. Soc. **62**, 1434 (2013).
[34] G. Zaránd, C.-H. Chung, P. Simon, and M. Vojta, Phys. Rev. Lett. **97**, 166802 (2006).
[35] O. M. Yevtushenko and V. I. Yudson, Phys. Rev. Lett. **120**, 147201 (2018).
[36] M. A. Ruderman and C. Kittel, Phys. Rev. **96**, 99 (1954).
[37] T. Kasuya, Prog. Theor. Phys. **16**, 45 (1956).
[38] K. Yosida, Phys. Rev. **106**, 893 (1957).
[39] N. Grewe and F. Steglich, in *Handbook on the Physics and Chemistry of Rare Earths*, edited by K. A. Gschneidner, Jr. and L. Eyring (North-Holland, Amsterdam, 1991), Vol. 14, p. 343.
[40] S. Doniach, Physica B+C **91**, 231 (1977).
[41] O. Stockert and F. Steglich, Annu. Rev. Condens. Matter Phys. **2**, 79 (2011).
[42] A. Nejati, K. Ballmann, and J. Kroha, Phys. Rev. Lett. **118**, 117204 (2017).
[43] B. A. Jones and C. M. Varma, Phys. Rev. B **40**, 324 (1989).
[44] B. Jones, Physica B **171**, 53 (1991).
[45] J. B. Silva, W. L. C. Lima, W. C. Oliveira, J. L. N. Mello, L. N. Oliveira, and J. W. Wilkins, Phys. Rev. Lett. **76**, 275 (1996).
[46] L. Zhu and J.-X. Zhu, Phys. Rev. B **83**, 195103 (2011).
[47] S. Nishimoto, T. Pruschke, and R. M. Noack, J. Phys.: Condens. Matter **18**, 981 (2006).
[48] A. Ramires and P. Coleman, Phys. Rev. B **93**, 035120 (2016).
[49] O. Sakai and Y. Shimizu, J. Phys. Soc. Jpn. **61**, 2333 (1992).
[50] T. Jabben, N. Grewe, and S. Schmitt, Phys. Rev. B **85**, 165122 (2012).
[51] I. Affleck, A. W. W. Ludwig, and B. A. Jones, Phys. Rev. B **52**, 9528 (1995).
[52] R. M. Fye, Phys. Rev. Lett. **72**, 916 (1994).
[53] B. Lechtenberg, F. Eickhoff, and F. B. Anders, Phys. Rev. B **96**, 041109 (2017).
[54] K. G. Wilson, Rev. Mod. Phys. **47**, 773 (1975).
[55] H. R. Krishna-murthy, J. W. Wilkins, and K. G. Wilson, Phys. Rev. B **21**, 1003 (1980).
[56] H. R. Krishna-murthy, J. W. Wilkins, and K. G. Wilson, Phys. Rev. B **21**, 1044 (1980).
[57] R. Bulla, T. A. Costi, and T. Pruschke, Rev. Mod. Phys. **80**, 395 (2008).
[58] J. R. Schrieffer and P. A. Wolff, Phys. Rev. **149**, 491 (1966).
[59] B. Lechtenberg and F. B. Anders, Phys. Rev. B **90**, 045117 (2014).
[60] L. Borda, Phys. Rev. B **75**, 041307 (2007).
[61] R. Bulla, T. Pruschke, and A. C. Hewson, J. Phys.: Condens. Matter **9**, 10463 (1997).
[62] D. C. Langreth, Phys. Rev. **150**, 516 (1966).
[63] F. B. Anders, N. Grewe, and A. Lorek, Z. Phys. B Condens. Matter **83**, 75 (1991).
[64] B. Lechtenberg, Equilibrium and nonequilibrium dynamics close to impurity quantum phase transitions, Ph.D. thesis, TU Dortmund, 2016.
[65] L. Zhu and C. M. Varma, arXiv:cond-mat/0607426.
[66] Z. M. M. Mahmoud, J. Bünemann, and F. Gebhard, Phys. Status Solidi (b) **254**, 1600842 (2017).
[67] J. M. Luttinger and J. C. Ward, Phys. Rev. **118**, 1417 (1960).
[68] T. Jabben, N. Grewe, and S. Schmitt, Phys. Rev. B **85**, 045133 (2012).
[69] R. Žitko and J. Bonča, Phys. Rev. B **74**, 045312 (2006).
[70] B. Lechtenberg and F. B. Anders, Phys. Rev. B **98**, 035109 (2018).
[71] M. I. Katsnelson and A. I. Lichtenstein, Phys. Rev. B **61**, 8906 (2000).
[72] L. Zhou, J. Wiebe, S. Lounis, E. Vedmedenko, F. Meier, S. Blügel, P. H. Dederichs, and R. Wiesendanger, Nat. Phys. **6**, 187 (2010).
[73] A. Allerdt, C. A. Büsser, G. B. Martins, and A. E. Feiguin, Phys. Rev. B **91**, 085101 (2015).
[74] D. N. Aristov and S. V. Maleyev, Phys. Rev. B **56**, 8841 (1997).
[75] R. Masrour, A. Jabar, A. Benyoussef, and M. Hamedoun, J. Magn. Magn. Mater. **401**, 695 (2016).
[76] K. V. Nefedev, V. I. Belokon, V. Yu. Kapitan, and O. I. Dyachenko, J. Phys.: Conf. Ser. **490**, 012163 (2014).
[77] S. Saremi, Phys. Rev. B **76**, 184430 (2007).
[78] T. Linneweber, J. Bünemann, Z. M. M. Mahmoud, and F. Gebhard, J. Phys.: Condens. Matter **29**, 445603 (2017).